A REAL-TIME LUCIFERASE ASSAY USING RECOMBINANT VESICULAR STOMATITIS VIRUS TO STUDY ENTRY OF HEMORRHAGIC FEVER VIRUSES

by

MARIA FERNANDA LAY MENDOZA

(Under the Direction of Melinda Brindley)

ABSTRACT

Since viral hemorrhagic fever (VHF) viruses such as Lassa virus (LASV) and Ebolavirus (EBOV) are classified as biosafety level 4 (BSL-4) pathogens, research with these viruses are limited. However, the glycoprotein is sufficient to study entry and can be performed in BSL-2 facilities. Here we constructed recombinant vesicular stomatitis viruses (rVSV) expressing the LASV and EBOV glycoprotein to monitor luciferase expression real-time during infection. This assay can be useful to study entry kinetics into cells in the presence or absence of receptors/attachment factors rendering high sensitivity, low background, and flexible experimental procedures with quick outputs. One limitation of this assay is that the bullet-shaped morphology of VSV is unique and distinct from most viruses, therefore, studying endocytosis pathways may not reflect those used by the authentic viruses.

INDEX WORDS: vesicular stomatitis virus, Ebola, Lassa, real-time, entry, luciferase

A REAL-TIME LUCIFERASE ASSAY USING RECOMBINANT VESICULAR STOMATITIS VIRUS TO STUDY ENTRY OF HEMORRHAGIC FEVER VIRUSES

by

MARIA FERNANDA LAY MENDOZA

BS, Penn State University, 2015

A Thesis Submitted to the Graduate Faculty of The University of Georgia in Partial Fulfillment of the Requirements for the Degree

MASTER OF SCIENCE

ATHENS, GEORGIA

2020

© 2020

MARIA FERNANDA LAY MENDOZA

All Rights Reserved

A REAL-TIME LUCIFERASE ASSAY USING RECOMBINANT VESICULAR STOMATITIS VIRUS TO STUDY ENTRY OF HEMORRHAGIC FEVER VIRUSES

by

MARIA FERNANDA LAY MENDOZA

Major Professor:	Melinda Brindley
Committee:	Mark Tompkins
	Maricarmen García

Electronic Version Approved:

Ron Walcott
Interim Dean of the Graduate School
The University of Georgia
August 2020

DEDICATION

To my father, whose unconditional love and support always encourages me to reach as far as I want; my four sisters whom I love dearly and always believed in me; my nieces and nephews, because their videos always relieved me from stress; my mother for spoiling me; and finally, my husband, who was always by my side during hardship and kept telling me how great I am.

ACKNOWLEDGEMENTS

To Dr. Melinda Brindley for her patience, trust, and positivity, thanks for your amazing mentoring and for believing in me. The Brindley Lab, especially Marissa, Kerri, and Blanka for helping inside and outside of lab. My undergraduate students Chris and Courtney for all your help reducing my workload. To the He Lab for allowing us to borrow materials and equipment as well to my committee members Dr. Mark Tompkins and Dr. Maricarmen Garcia for their help and patience.

TABLE OF CONTENTS

Page

LIST OF FIGURES

Page

CHAPTER 1

INTRODUCTION

Significance

Viral hemorrhagic fever includes a group of zoonotic illnesses characterized by vascular damage affecting multiple organs. Viruses from four different RNA families are known to cause VHF: *Filoviridae, Arenaviridae*, *Bunyaviridae,* and *Flaviviridae.* Several viruses within these families are classified as BSL-4 pathogens, limiting their study in conventional BSL-2 facilities. Symptoms are virus-specific but generally include fever, muscle pain, malaise, headache, vomiting, and diarrhea; and vary from mild to life-threatening. Severe cases manifest with internal bleeding and multiorgan failure which can be fatal. The natural reservoirs for VHF viruses vary from a wide array of arthropods and vertebrates that inhabit several locations around the world, thus making VHF a global concern (**figure 1.1**) [1].

As viruses are obligate intracellular parasites, entry into a cell is crucial to successfully establish infection in the host. Understanding cellular-viral interactions that mediate entry into a host, can help us gain insight into the virus' cellular-, tissue-, and host tropism, to ultimately aid in the development of preventative and counter measures. As a lab that focuses on researching viral entry, we want to develop an assay that will allow us to study entry mechanisms of enveloped viruses and detect specifically fusion pore formation events in real time.

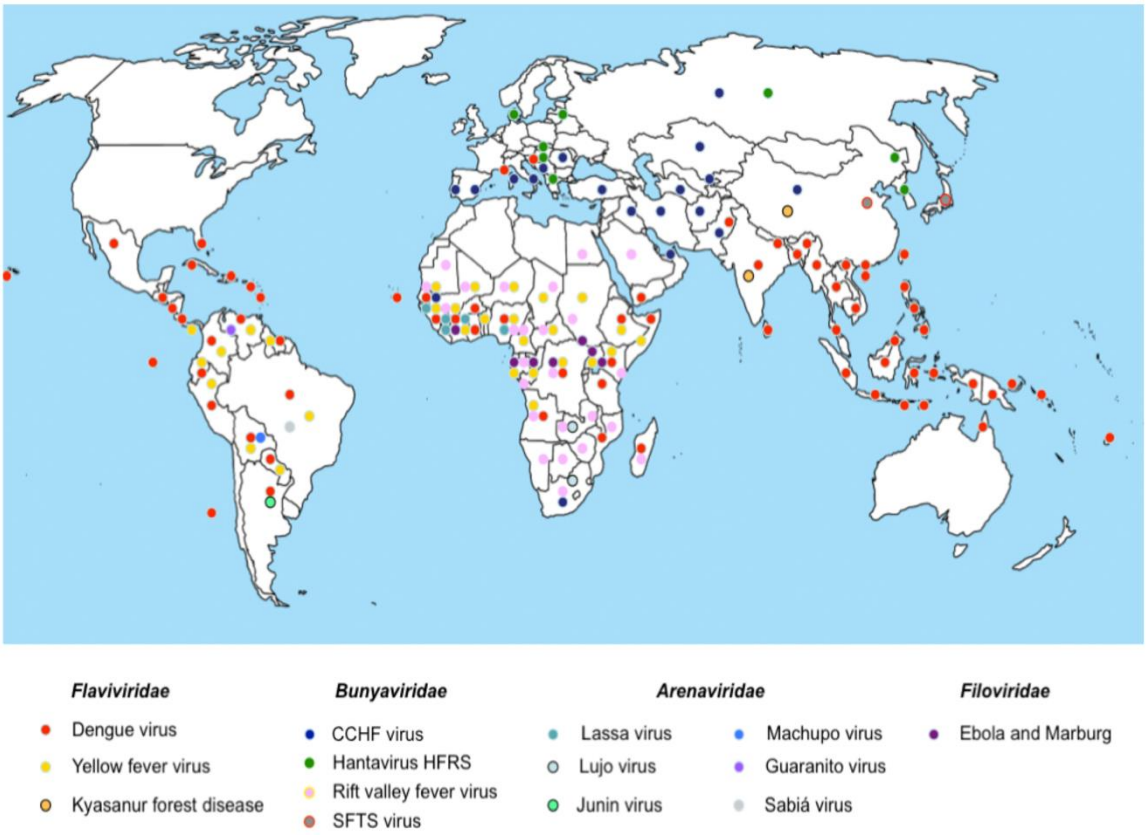

Figure 1.1. Global distribution of viruses that cause viral hemorrhagic fever. VHF can be caused by viruses from the *Flaviviridae*, *Bunyaviridae*, *Arenaviridae*, or *Filoviridae* families. The map above shows the geographical distribution around the globe of viruses pertaining from the four different families. Figure was borrowed form Zapata et al., *Plos Neglected Tropical Diseases*, 2014. No alterations have been made (back).

CHAPTER 2

LITERATURE REVIEW

Endocytosis

Viruses can utilize several entry pathways to enter host cells, which typically involve endocytic uptake of viral particle by the cell [2,3]. Endocytosis is a mechanism cells use to internalize extracellular material by capturing them in a portion of plasma membrane, which is then released into the cytoplasm as an endosome. Endocytic vesicles either recycle back to the plasma membrane or are shuttled through the endosomal pathway, usually via the early endosome. The early endosome is a transient and distinct organelle located at the periphery of cell, holds a pH of 6.5-6.0, and functions as a sorting complex. As endosomes mature and move to the perinuclear space, they become larger and more acidic. Ultimately, maturing endosomes fuse with lysosomes for degradation of contents (**figure 2.1**) [4,5].

Major pathways shown to be important in viral entry are macropinocytosis, clathrin-, and caveola-mediated endocytosis (**figure 2.2**). Macropinocytosis is defined as the nonspecific uptake of extracellular fluid and large solutes. Uptake can be stimulated by growth factors [6-8] which signal actin polymerization at the membrane to promote ruffling and formation of macropinosomes [9]. However, antigen-presenting cells (APCs) do not require signaling and are capable of constitutive macropinocytosis [10]. Macropinosomes are uncoated vesicles greater than 0.2 μm in diameter [9] and form in approximately 10 minutes [11]. Amilorides and derivatives such as eicosapentaenoic acid (EIPA) are known

to specifically inhibit macropinocytosis by blocking the Na^+/H^+ Exchanger (NHE), ultimately preventing membrane ruffle [12].

Clathrin-mediated endocytosis is the major endocytosis pathway in many cell types [13]. Cargo signals sequential recruitment of over 50 adaptors [14,15] to coat the growing membrane pit, which grows to 60-120 nm in diameter. Upon complete formation, a cellular scission protein, known as dynamin, releases the coated vesicle from the plasma membrane. The whole process occurs within 1-2 minutes from *de novo* clathrin-coated vesicle formation to pinching off of the plasma membrane by dynamin [15]. Chlorpromazine is a psychotic drug used to treat schizophrenia and widely use to inhibit clathrin-mediated endocytosis because it interferes with assembly and disassembly of clathrin latices [16].

During caveolae-mediated endocytosis, “little caves” of 50-80 nm in diameter are formed from rigid microdomains rich in cholesterol and caveolins, an integral membrane protein [17]. Because only 2% of formed caveolin-positive vesicles buds per minute [18], caveolae are considered less dynamic and very slow. Therefore, it has been proposed that the major role of caveola-mediated endocytosis is for lipid transport and to maintain membrane integrity [19,20]. Nystatin is widely used to study caveola-mediated endocytosis as it depletes membrane cholesterol thus, interfering with this process [21].

Dynasore is another entry inhibitor commonly used to block dynamin activity, thus preventing the scission of endocytic vesicles from the plasma membrane, both clathrin- and caveola-mediated endocytosis are susceptible to inhibition [22,23].

Viral membrane fusion proteins

Enveloped viruses must fuse with a cellular membrane to deliver their genome into a target cell. Membrane fusion is thermodynamically favorable but must overcome an energy barrier due to repulsive hydration forces [24]. Through a hemi-fusion state, viral fusion proteins catalyze this reaction by providing free energy from conformational changes [25] triggered by low pH and/or protein interactions. Enveloped viruses must have at least one envelope protein to induce membrane fusion; in some instances, the same protein also mediates receptor binding and in other cases, a second protein functions in cell attachment. Membrane fusion must occur with all enveloped viruses which come from very distinct families and naturally, their fusion proteins differ greatly in their amino acid sequence. Nonetheless, most characterized fusion proteins fall within one of the existing three classes discussed below [26].

The pre-fusion state of class I fusion proteins consists of a homotrimer of coiled α-helices. All characterized class I fusion proteins (ex. *Filoviridae* and *Arenaviridae* 's GP2) must be converted from a fusion-incompetent to a fusion-competent state by priming. Priming entails proteolytic cleavage, which can occur during the secretory pathway, in the Golgi apparatus or the endoplasmic reticulum (ER), the plasma membrane, or in endosomes during entry [26,27]. Class II fusion proteins (ex. *Togaviridae*'s E1) are characterized by dimers of β-sheets running parallel to the lipid bilayer and require priming as well. Class III fusion proteins (ex. *Rhabdoviridae*'s G and *Herpesviridae*'s gB) contain both α-helices and β-sheets structures and do not require priming [26,27]. All fusion proteins undergo an irreversible conformational change from its pre-fusion state to a trimer-of-hairpins post-fusion state (**figure 2.3.a-c**) [26,28]. The Rhabdovirus and

Baculovirus glycoproteins (G and gp64, respectively) are the only exception to this rule; because controlling the pH can revert the post-fusion conformation back to the pre-fusion state of the glycoproteins and restore infectivity of Rhabdoviruses [29]. In the case of gp64, even though the protein is able to revert to the pre-fusion conformation, the virus infectivity is irreversibly inactivated upon exposure to low pH [30].

There are four basic mechanisms that trigger fusion a) by receptor interaction, b) exposure to low pH, c) by receptor interaction then exposure to low pH, or d) by receptor interaction and then protease cleavage. The type of fusion trigger is generally not constrained to the class of fusion protein or to the viral family, although, some families do employ the same mechanism (ex. Flaviviruses are triggered upon low pH). Fusion can occur in any compartment of the endosomal pathway, depending on protein interaction and pH requirements; it is virus-specific and generally irrespective of the class of fusion protein as well [28].

Vesicular stomatitis virus

VSV belongs to the *Rhabdoviridae* family and is the causative agent of a livestock illness similar to foot-and-mouth disease (FMD) [31]. Infected animals primarily transmit the virus within herds via direct contact and fomites, although several species of insects play an important role as vectors as well. Defining a natural reservoir is problematic because the virus can infect a wide range of species [32]. There are two major serotypes in the United States, New Jersey and Indiana. The incubation period is 2-8 days before symptoms manifest after contracting the virus. Symptoms include but are not limited to oral- and/or udder blisters, anorexia, and lethargy. There is no treatment, but the disease is self-limiting and lasts about 2 weeks [33]. Even though VSV can infect a wide range of

mammals and insects, it is only a major concern for farmers due to economic losses. Humans tend to be asymptomatic, with the occasional development of mild flu-like illness and oral lesions, and extremely rare cases of encephalitis in infants [34]. The disease is only endemic in Central and South America and there are rarely any cases in the United States, however, it is a reportable disease. While rare, new outbreaks were detected in the U.S. with 60 cases in April 2020 and 1,144 cases in 2019 in equine and bovine species. Prior to the 2019 outbreak, the last documented outbreak of VSV happened in 2006 [33].

The VSV genome is a single-stranded negative sense RNA molecule. It is 11,161 base pairs long containing 5 genes which encode for 5 proteins sequentially produced: nucleoprotein (N), phosphoprotein (P), matrix protein (M), envelope glycoprotein (G), and an RNA-dependent RNA polymerase (L). All 5 proteins are present within the viral particle [32]. Virions have a distinct bullet-shaped morphology typically measuring 180 nm long and 65 nm width [35].

The glycoprotein is the only protein found on the exterior of the virion; it is produced as a single polypeptide, and the pre-fusion conformation consists of a non-covalently linked homotrimer which is responsible for both receptor recognition and fusion with host membranes (**figure 2.4.a**) [36].

VSV can infect almost any cell except unstimulated B-, T-, and $CD34^+$ cells. The low-density lipoprotein receptor (LDL-R) has been suggested to be the cellular receptor for VSV as it is produced in susceptible cells, but lacking on non-susceptible cells [37,38]. Once VSV engages the cellular receptor at the plasma membrane, it is internalized through an “incomplete” clathrin-mediated endocytosis [39-42]. The particle morphology is too long to fit in a classic clathrin-coated pit and requires additional actin rearrangement to

complete the process. Once within an endosome, low pH induces protein G conformational changes in the early endosome to induce fusion between 2 to 10 minutes after internalization [42-44].

Molecular biology techniques enabled the first recovery of infectious VSV particles from a DNA plasmid 25 years ago [45,46]. Because VSV has a negative sense genome, transfecting the genome into cells is not sufficient to produce virus. Four plasmids are required, expression vectors producing the protein components of the RNA-dependent-RNA polymerase (N, P and L) in addition to a plasmid encoding the viral genome. The viral genome is produced by a T7 polymerase, so it lacks the 5' cap added by cellular polymerase II. Once the full-length DNA copy of the genome was placed in a plasmid, various alterations could be tested. It was quickly recognized that the glycoprotein could be removed from the genome as long as the protein was supplied *in trans* by a plasmid [47]. Furthermore, it was recognized that other viral glycoproteins could be incorporated onto the VSV particles and mediate entry [48]. Even replication competent VSV in which the for foreign glycoprotein replaces the VSV G in the genome can be recovered. These recombinant viruses have been used extensively to study the entry of viruses that typically require high containment, such as EBOV and LASV. They have also been used as vaccine vectors. On December 19, 2019, the FDA approved an Ebola virus vaccine in a rVSV vector containing the EBOV glycoprotein of the Zaire species (rVSV/ZEBOV), under the trademark Ervebo. rVSV appears to be a safe and effective vector due to the virus being low risk in humans and demonstrating low seropositivity in the human population, with the exception of certain groups such as farmers, laboratory workers, and veterinarians [49].

Lassa mammarenavirus

LASV causes VHF through human contact with rodent reservoirs, *Mastomys natalensis* [50,51] commonly via household infestations, where food is stored, through aerosol inhalation of rodent urine during cleaning and person-to-person transmission through direct contact. These rodents inhabit countries in West Africa including Sierra Leone, Liberia, Guinea and Nigeria, where Lassa Hemorrhagic Fever (LHF) is endemic [52]. LHF was first described in the 1950s, however, it was not until 1969 when the virus was identified in Nigeria; and was named after the town where it was first identified [53].

It is estimated that 100,000-300,000 cases occur yearly [54], with 5,000 deaths. While 80% of infections are asymptomatic, symptoms appear in 20% of cases 2 to 21 days after getting infected by the virus. Symptoms vary from mild to severe. Severe cases include internal bleeding and multiorgan failure. Deafness is a common sequelae of LASV infection regardless of symptom severity and occurs in 25% of symptomatic cases. Lassa-induced deafness can be permanent, but in some cases hearing returns within 3 months [55,56]. There are no vaccines available to prevent the Lassa virus infection, but can be controlled by Ribavirin if administered early in infection [57], although it is not officially licensed to do so.

LASV is a pleomorphic virus measuring about 70 – 150 nm in diameter, which is common among arenaviruses [58,59]. It contains two negative single-stranded RNA genomes, the L and the S segment, encoding four structural proteins [60]. The L segment is 7.5 kb and encodes for the polymerase (L) [61] and the matrix protein (Z) [62]; and the S segmented is 3.5 kb and encodes for the surface glycoprotein (GPC) and the

Nucleoprotein (N) [61,63]. Both segments encode for the two proteins in an ambisense fashion [64].

The surface glycoprotein is synthesized as a single polypeptide and undergoes two proteolytic events. In the endoplasmic reticulum (ER) the signal peptide is cleaved by signal peptidase and in the Golgi apparatus the proprotein convertase Subtilisin Kexin Isozyme-1/site-1 protease (SKI-1/S1P) cleaves GP1 from GP2 [65-67]. The mature prefusion form is a trimer of SSP/GP1/GP2 noncovalently associated (**figure 2.4.b**). [68]. Each monomer has 11 N-linked glycosylation sites which together comprises 25% of the total mass within the trimer. The glycans are important for immune evasion, as well as GPC transport and processing [69,70]. The SSP is a long transmembrane stable signal peptide essential for intracellular transport and GPC maturation and fusion [71-74]. SSP has been shown to be important for Lymphocytic choriomeningitis virus (LCMV) infectivity, the prototypic virus of the *Arenaviridae* family [67,75]. GP1 is a 42-44 kDa subunit that engages with cellular receptor [76] and GP2 is a 36-38 kDa subunit responsible for mediating membrane fusion [77].

The major cellular receptor for LASV is α-dystroglycan (αDG) [78]. It requires glycosylation by glycosyltransferase LARGE1 for efficient attachment of LASV GPC to occur [79]. Dystroglycan (DG) is encoded by the *DAG1* gene and is cleaved post-translationally into the extracellular domain αDG and intracellular domain βDG. αDG naturally binds laminin and βDG binds dystrophin. DG functions as a linker of the extracellular matrix to the cytoskeleton in many skeletal muscle tissues [80].

In the absence of functional αDG, other receptors/attachment factors mediate entry of LASV. These include a) glycosaminoglycan (GAG) heparan sulfate [81], b) C-type

lectins dendritic cell-specific intracellular adhesion molecule-3-grabbing nonintegrin (DC-SIGN) [82] and liver and lymph node sinusoidal endothelial calcium-dependent lectin (LSECtin) [83], and c) phosphatidylserine (PS) receptors Axl and Tyro3 from the Tyro3/Axl/Mer (TAM) receptor family kinases [83,84], and T-cell immunoglobulin and mucin domain 1 (TIM-1) [85].

LASV has been reported to enter cells via a clathrin-mediated endocytosis [86], However, other studies suggest entry involves a macropinocytosis-like pathway [87-89]. Once endocytosed, low pH induces GPC conformational changes and a GP1 receptor switch to lysosomal associated membrane protein 1 (LAMP1) within the late endosome to initiate fusion [81,90].

Ebolavirus

Ebola virus disease (EVD), another type of VHF, is a rare but often fatal illness that affects humans and nonhumans primates. The natural reservoir for EBOV has been suggested to be fruit bats [91-93]. The disease is characterized by hemorrhagic fever and flu-like symptoms, and manifest 2 to 21 days after contracting the virus. EBOV spreads from person-to-person through direct contact with body fluids of an infected person or contaminated objects, and case fatality rates range from 25% to 90%. On December 19th, 2019, the FDA approved a vaccine under the tradename Ervebo [94-96].

The first reported case of EVD in 1976 appeared simultaneously in 2 different locations, in Nzara, Sudan caused by Sudan ebolavirus and in Yambuku, Democratic Republic of Congo caused by Zaire ebolavirus. The latter is responsible for most and recent outbreaks that repeatedly occur in West Africa. The largest outbreak recorded is the 2014-2016 outbreak in Sierra Leone, Libera, and Guinea, with about 28,600 total cases and

11,325 deaths. The most recent outbreak started in 2018 in The Democratic Republic of Congo (DRC) and was finally declared over in June 2020, resulting in more than 3,444 reported cases and at least 2,264 deaths [95,96]. More than 300,000 doses of the Ervebo vaccine were administered during the 2018 DRC outbreak. Before the resolution of the 2018 outbreak, a second EBOV outbreak was detected in the DRC, unrelated to the previous one.

EBOV is a long, filamentous, enveloped virus; measuring on average 900 nm in length and 80 nm in width, however, particles as long as 14 µm in length have been reported with up to 22 genome copies per particle [97-99]. The 19-kb genome is a negative sense single-stranded RNA; there are 7 genes encoding for 7 structural proteins [100] and 2 non-structural proteins [101-104].

The GP gene produces 3 different mRNA transcripts resulting in 3 different versions of GP. The primary transcript is soluble GP (sGP) which accounts for 70% of the protein product [104], and is thought to function immune evasion by acting as a decoy [105]. Small secreted GP (ssGP) accounts less than 5% of the product and is produced as result of co-transcriptional editing from two adenosine insertions, its function is unknown [104]. Both proteins are identical to the first 295 amino acids of the N-terminus of GP, but lack the transmembrane domain [101,102]. Lastly, membrane bound GP is also produced from co-transcriptional editing from insertion of one adenosine only [101,102]. The GP0 precursor is cleaved by furin to yield the GP1 ectodomain (130 kDa) and the GP2 transmembrane domain (24 kDa) [106,107]. The final conformation is a 450 kDa trimer composed of GP1/GP2 heterodimers [108] held together by disulfide bonds (**figure 2.4.c**) [109]. While GP2 contains the fusion loop, GP1 consists of the receptor-binding domain

with both N- and O- linked glycans. The linked glycan cap is required for immune evasion [110] and efficient interaction with C-type lectins attachment factors [111] and the O-linked glycosylated mucin-like domain (MLD) is involved in pathogenicity [112]. Other post-translational byproducts include shed GP and Δ-peptide. Shed GP is produced by the cleavage of GP ectodomain by the cellular metalloprotease Tumor Necrosis Factor-α converting enzyme (TACE). Shed GP is secreted from infected cells, binds neutralizing antibodies, and induces a cytokine storm by activating non-infected macrophages and dendritic cells, thus, contributing to pathogenesis [113,114]. The Δ-peptide is a small product thought to be a viroporin and permeabilize the cellular membrane [115-117].

The first cellular targets of EBOV are dendritic cells and macrophages, which then spread the infection to several parts of the body including the liver, kidney, spleen, etc., causing multiorgan failure and ultimately death [118]. No specific high-affinity entry receptors have been identified. However, numerous attachment factors can help facilitate entry into several types of cells such as heparan sulfate [119]; C-type lectins: DC-SIGN, liver/lymph node-specific ICAM-3 grabbing non-integrin (L-SIGN), LSECtin, and human macrophage C-type lectins specific for galactose/*N*-acetylgalactosamine (hMGL) [111,120-123]; β-1 integrins [124]; and PS receptors: TIM-1 and -4 and TAMs [125-128].

Ebola primarily enters cells via macropinocytosis, likely through apoptotic mimicry [129-132]. Clathrin- and caveolae-dependent endocytosis have also been observed in different cell types with alternative models used to study EBOV entry [133-135] although these studies have been disputed [136,137]. Once within an endosome, EBOV GP requires proteolysis by cathepsins B and L [137-139] for priming in order to interact with the

cholesterol transporter Niemann-Pick C1 (NPC-1), and trigger fusion in a pH-dependent manner in the endolysosome [140-142].

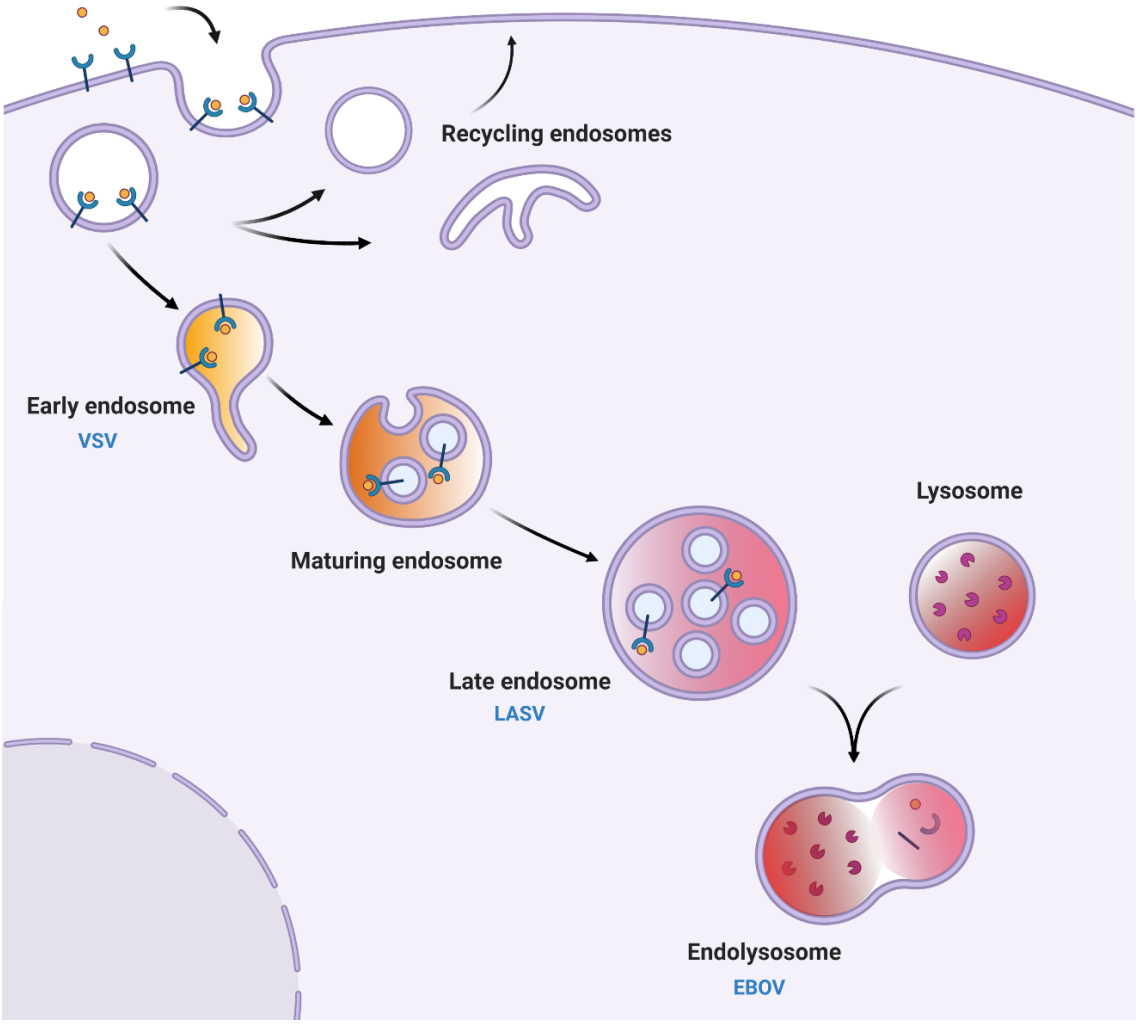

Figure 2.1. Endosomal trafficking pathway. Upon endocytosis, cargo can recycle back the plasma membrane via a fast- or slow-recycling process. Alternatively, endosomes can be shuttled through the endosomal trafficking pathway generally via the early endosome, depending on the cell type. The early endosome holds a pH of 6.5-6.0, and functions as a sorting complex. As early endosomes mature, they become larger and more acidic and gain stage-specific markers. Relative pH is shown as a color gradient (yellow less acidic to red more acidic). The ultimate fate of maturing endosomes is fusion with lysosomes for degradation. Shown in blue text are sites where different viruses fuse with the endosomal membrane. Figure was created in BioRender (back).

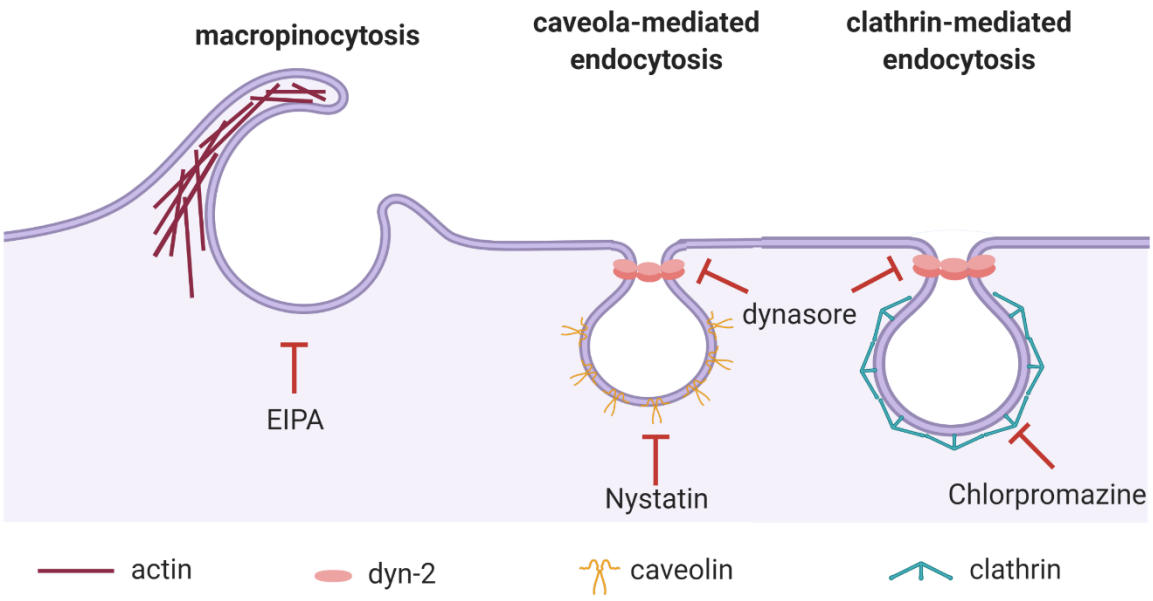

Figure 2.2. Major endocytic pathways important for viral entry and inhibitors. Macropinocytosis (left) relies heavily on actin polymerization and is constitutively active on APCs, while on non-APCs can be activated by growth factors. Caveolae-mediated endocytosis (center), a cholesterol- and caveolin-dependent mechanism happens at a slow rate. Clathrin-mediated endocytosis (right) is a fast process happening within 2 minutes, it is the major mechanism of endocytosis in general for several cells for cargo internalization. Figure was created in BioRender (back).

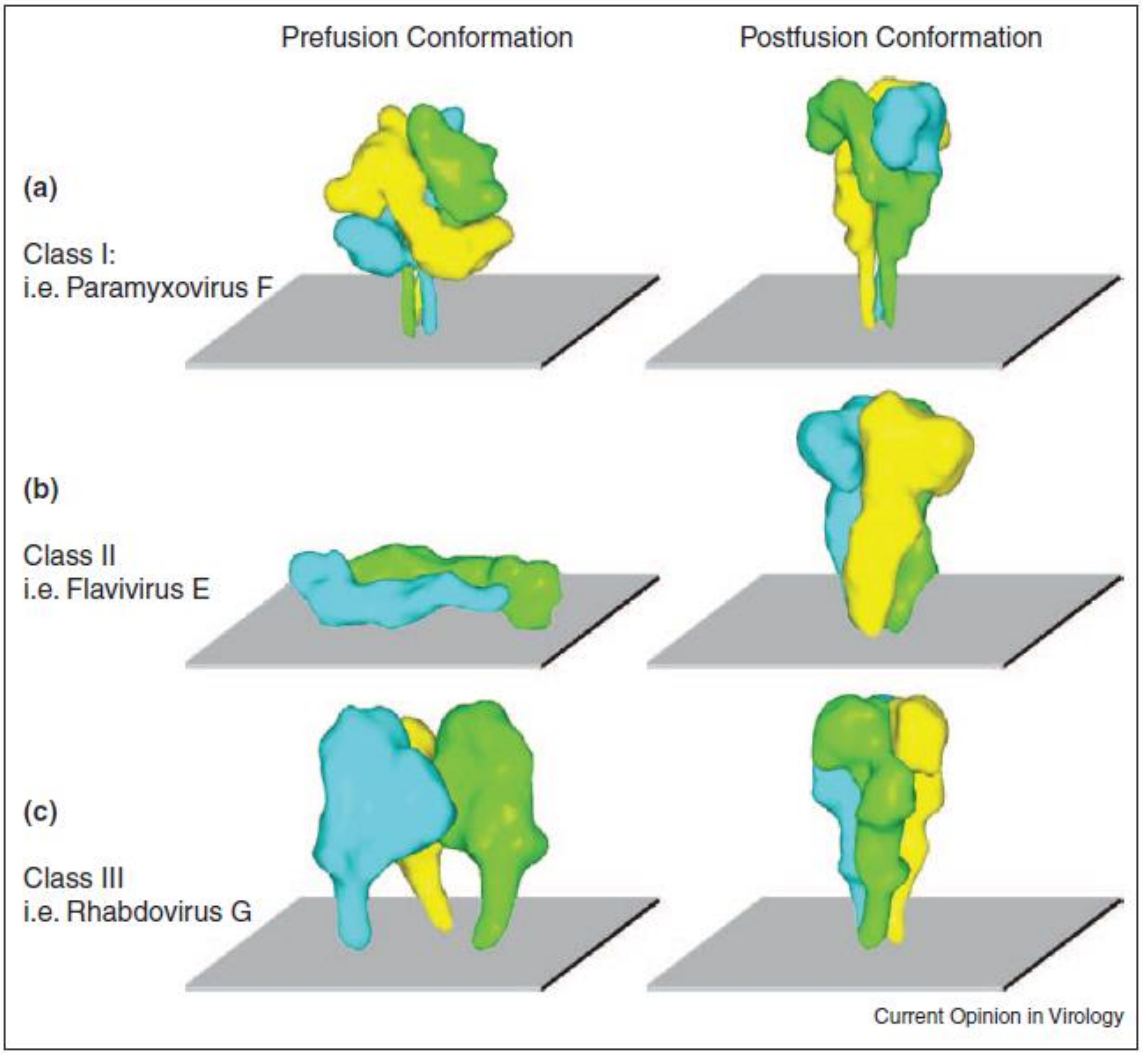

Figure 2.3. Classes of viral fusion proteins. Prefusion conformations of **a)** class I fusion proteins, consisting of homotrimers of coiled α-helices. **b)** class II fusion proteins made by a dimer of β-sheets running parallel to the plasma membrane. **c)** class III fusion proteins consisting of homotrimers containing mixed structures of α-helices and β-sheets. The post-fusion conformation, a trimer-of-hairpins, is shared by all class fusion proteins. Figure was borrowed from Plemper, *Curr Opin Virol*, 2010 and no modifications were made (back).

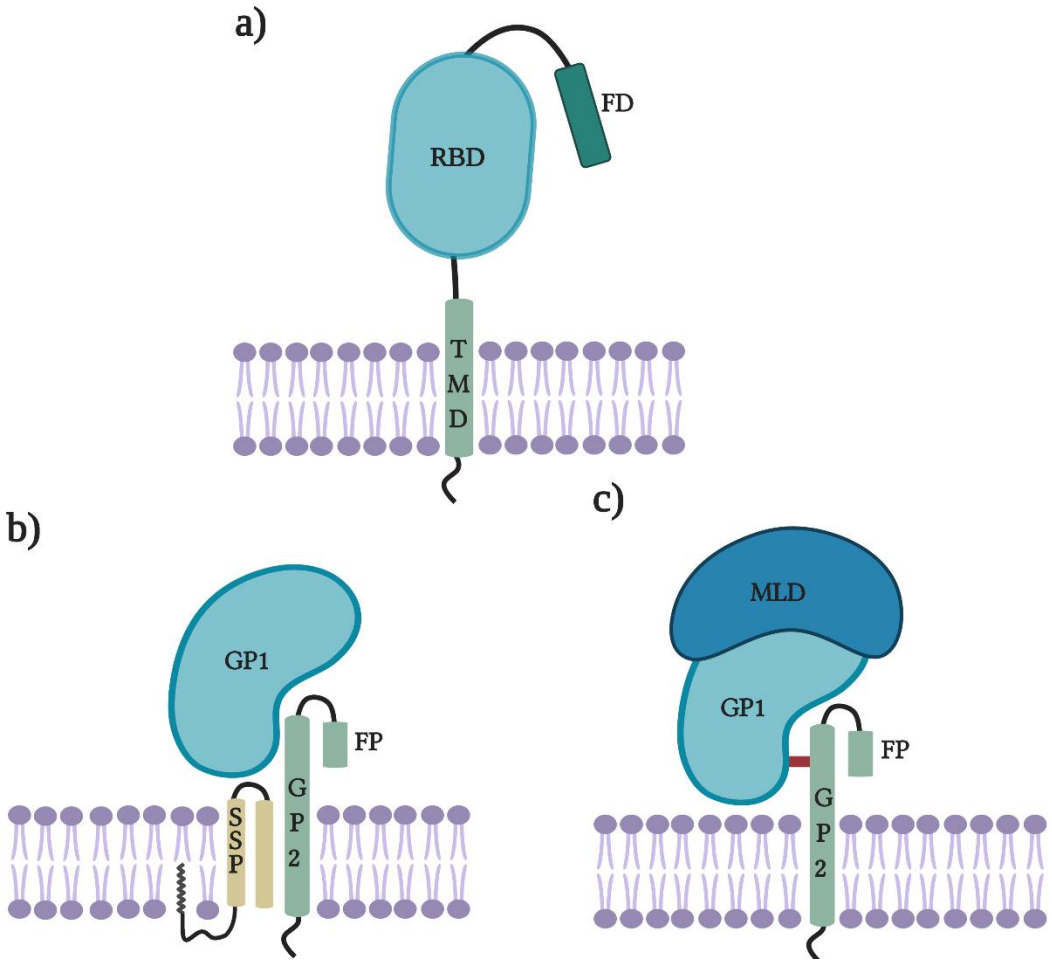

Figure 2.4. Simplified schematics of glycoprotein structures. The graphics above shows only the monomeric form of each glycoprotein. **a)** The VSV envelope is a homotrimeric glycoprotein non-covalently linked together. Each protomer has three domains: a transmembrane domain (TMD), a receptor-binding domain (RBD), and a fusion domain (FD) (back to VSV). **b)** The LASV envelope is a trimer of GP1/GP2/SSP heterotrimers non-covalently linked. GP1 contains the RBD and is heavily glycosylated, GP2 contains the TMD and the fusion peptide (FP), the SSP acts as a pH sensor and is also important for fusion. (back to LASV). **c)** The EBOV envelope is a heterotrimer of GP1/GP2 dimers linked together by disulfide bonds. GP1 contains the RBD, a glycosylated MLD; GP2 is the TMD and contains the FP. Figure was created with BioRender (back to EBOV).

CHAPTER 3

A REAL-TIME LUCIFERASE ASSAY USING RECOMBINANT VESICULAR STOMATITIS VIRUS TO STUDY ENTRY OF HEMORRHAGIC FEVER VIRUSES

Introduction

Enveloped viruses are covered in a lipid membrane acquired from infected cells. In order for enveloped viruses to infect naïve cells and deliver their genome, the virus must interact with the host cell and initiate a membrane fusion event between the viral envelope and a cellular membrane. To accomplish membrane fusion, viruses produce fusion proteins which are complicated little machines studded in the viral membrane. Several methods have been developed to study viral fusion including cell-cell and virus-cell fusion assays. The goal of my master's project was to develop a new virus-cell fusion assay to monitor and compare fusion in a biologically relevant system and in real-time.

Cell-cell fusion assays are based on an effector cell expressing the envelope glycoprotein and a target cell expressing the receptor. Cells are co-cultured, and syncytium can be induced upon exposure to low pH or protease treatment. While this system works well to monitor the fusion activity of viral glycoproteins that can be readily triggered, it by-passes the required endocytosis process that occurs during natural infection. Additionally, we have yet to determine the fusion trigger for some viral glycoproteins, such as EBOV, and therefore cell-cell fusion assays cannot be used.

Virus-cell fusion assays frequently utilize a retroviral core. Retroviral systems generally use human immunodeficiency virus (HIV) or murine leukemia virus (MLV) platforms to make pseudo-particles coated with the viral envelope of interest. Generally, pseudo-particle delivers a transcription factor to the target cell to induce expression of a reporter gene such as luciferase or the retroviral core includes a reporter such as β-lactamase. Some general disadvantages of these assays are high background, sensitivity, and reagent cost.

Previous efforts by our lab focused on developing a virus-cell entry assay that would detect fusion events in live cells by using a virus that incorporates Nanoluciferase (NLuc) within the viral particle. Once fusion occurs, the luciferase released by the virus would react with the substrate furimazine. Endurazine a is membrane permeable version of furimazine which must be hydrolyzed by cellular esterases to become active. Luciferase then catalyzes the oxidation of furimazine to convert it to furimamide while releasing light (**figure 3.1.a**). Unlike Firefly luciferase, Nanoluciferase does not require ATP for reaction catalysis and is 100X brighter than Renilla luciferase. Hence, background is reduced, and sensitivity improved. To achieve this, we cloned Nluc embedded into the M gene of VSV, so the matrix protein of the virus physically contains the luciferase enzyme [143]. When we tested this construct, unfortunately, the Promega substrate produced significant signal because it reacted with the luciferase embedded in the virion without cellular esterase activity, thus preventing us from monitoring fusion pore formation. However, this technique is still useful to monitor budding efficiency [143]. Therefore, for my thesis project we used a rVSV vector with the *Nluc* gene coded in the genome without packaging

the enzyme in the virion. Although we are not able to detect specific fusion events this technique can still be used to study entry real-time with Endurazine.

We produced four recombinant VSV (rVSV) with the glycoproteins of VSV, LASV, EBOV, and Chikungunya virus (CHIKV) and the Nluc gene in a post-envelope location (**figure 3.1.b**). We can use rVSV viruses to compare the entry kinetics of LASV and EBOV, because while this assay does not directly detect fusion events, standardizing the replication machinery across all viruses enables us to assume that differences in luciferase production are due to differences in entry kinetics. The assay readily detects cell permissiveness differences. We can also compare entry efficiency in the presence of endocytosis inhibitors and exogeneous (i.e. transiently expressed) attachment factors within one cell line. A limitation of this model is that particle morphology of VSV is radically distinct from authentic LASV and EBOV and, when studying endocytic pathways, virus morphology can greatly impact the pathway taken and not reflect the endocytic pathways used by authentic viruses.

Materials & methods

Cell lines and Transfection

Vero (Vervet kidney cells, previously known as African green monkey) constitutively expressing human SLAM/CDw150 (signaling lymphocytic activation molecule 1) [144] and Baby Hamster's Kidney cells (BHK21) stably expressing T7 RNA polymerase [145] were maintained in high glucose Dulbecco's Modified Eagle Medium (DMEM) supplemented with 5% FBS (vol/vol). Human Embryonic Kidney cells (HEK293) that express the SV40 large T antigen (kindly provided by Dr. Biao He from University of Georgia) were maintained in high glucose DMEM supplemented with 10%

FBS (vol/vol). Human Haploid HAP1 and HAP1-ΔDAG1 cells (Horizon Discovery) were maintained in Iscove's media supplemented with 8% FBS. All cells were kept at 37°C with 5% CO_2. BHK-T7 cell transfections were performed with GeneJuice (Millipore Sigma) and HEK293T cells were transfected with jetPRIME® (PolyPlus Transfection) according to the manufacturer's instructions.

Drugs, plasmids, and antibodies

Drugs used to inhibit endocytosis were EIPA, dynasore, nystatin, chlorpromazine hydrochloride (all from Millipore Sigma), dissolved in either dimethyl sulfoxide (DMSO) or water. Plasmids used to transfect HEK293Ts were pmax-GFP (Amaxa®) as control, pCS6-Axl (BC032229, TransOMIC,), pCS6-Tyro3 (BC051756, TransOMIC), TIM-1-GFP [125], or pCS6-L-SIGN (BC038851, TransOMIC). Primary antibodies used for immunoblots were against GAPDH (clone 0411, Santa Cruz Biotechnology, 1:2,000), Axl (#AF154, R&D Systems, 1:2,000), GFP (#A-6455, ThermoFisher, 1:1,000), Tyro3 (#AF859, R&D Systems, 1:1,000), and L-SIGN antibody (clone 2G1, ThermoFisher, 1:200).

Cloning of viruses

GFP from rVSV/EBOVGP-GFP and rVSV/VSVG-GFP molecular clones [143] were replaced with the Nluc gene (pNL1.2; Promega™) utilizing NheI and AvrII restriction sites. To produce pVSV/LASVGPC-Nluc and pVSV/CHIKVE-Nluc, the codon optimized protein coding region of LASV GPC (Josiah strain) [146] and CHIKV E (S27 strain) [147], a kind gift from Dr. Graham Simmons (University of California), were amplified with additional MluI and NheI sites which were used to clone into the molecular clone. Rescue of rVSV viruses was completed as previously described [143]. For

experiments, the initial recovered virus was passaged onto a T75 of Vero cells (P2 stocks) and in some instances the P2 stock was used to generate more virus (P3 stocks). Stocks and samples were titrated by serial diluting samples in media and determining the median tissue culture infectious dose ($TCID_{50}$) using the Spearman-Karber $TCID_{50}$ method [148]. For some experiment's stocks were titrated with plaque assay on Vero cells as previously described [149].

Immunoblots

To detect proteins expressed in HEK293T, cells were seeded in a 6-well plate at a confluency of 70%. The next day, cells were transfected with 2 µg of plasmid and cell lysates were collected 24 hours post-transfection. Transfected cells were pelleted (800 x g, 5 minutes), resuspended in 100 µl of 1X PBS, lysed with 100 µl M2 lysis buffer (50 mM Tris, pH 7.4, 150 mM NaCl, 1 mM EDTA, 1% Triton X-100) and cleared of insoluble material (17,000 x g, 30 min, 4°C). Cell lysates were denatured in SDS-UREA buffer (200 mM Tris, pH 6.8, 8 M urea, 5% sodium dodecyl sulfate (SDS), 0.1 mM EDTA, 0.03% bromophenol blue, 1.5% dithiothreitol) for 30 minutes at 56°C, separated on an 4-20% Tris-Glycine SDS-PAGE gel (Invitrogen) and transferred to polyvinylidene difluoride PVDF membranes. Membranes were incubated with aforementioned primary antibodies, corresponding secondary antibodies conjugated with Horse-radish peroxidase (HRP) were used to detect the proteins. Protein signals were detected with West Dura (ThermoFisher) and imaged on a BioRad ChemiDocXRS (Bio-Rad).

Live luciferase assays

Cells were seeded in a black-walled clear bottom 96-well plate one or two days before the assay. Cells were infected with one of the rVSV-Nluc viruses at the indicated

multiplicity of infection (MOI) in the presence of Endurazine substrate (Promega™). When examining luciferase production in multiple cell lines, in the presence of drug, or transfected cells, both Endurazine and viral inoculum were present for the length of the experiment. In other assays, the media was replaced to remove inoculum and substrate before measuring luminescence. Luciferase activity was measured every 10 minutes at 37°C with a Glomax® Explorer (Promega™).

Replication Curves

Vero cells were seeded at a density of $2.0x10^5$ cells/well in 12-well plates and incubated for 48 hours. Cells were infected with the specified virus at a MOI of 0.01 PFU/cell for 1 hour at 37°C. Media was refreshed and virus was collected at times 0 (immediately), 4, 8, 12, 18, 24, and 48 hours after media replacement. Samples were diluted and tittered via $TCID_{50}$ on Veros cells.

Results

Kinetics of rVSV/VSVG Luciferase Expression

To examine how quickly we can detect luciferase production from the rVSV system, we first observed rVSV/VSVG because VSV G is known to quickly enter cells and fuse out of early endosomes [42]. We first assessed how changes in MOI values could impact the kinetics of rVSV/VSVG luciferase expression, by infecting Veros at a MOI of 25, 5, 1, 0.2, and 0.04 PFU/cell. Substrate was preincubated with cells for an hour, then virus was added to the cells for one hour as well. Both the inoculum and luciferase substrate were removed, and the plate was placed in a warmed plate reader. This ensured that only particles that bound and internalized within the hour could initiate infection. At 1-hour post-infection, cells infected with a MOI of 25 displayed a luciferase signal value of

~10,000 units and quickly peaked 3 hours post-infection. At a MOI of 5, the luciferase signal was relatively higher than that of background levels (not appreciable from the figure) and its peak was observed at 4 hours post-infection (**figure 3.2.a**). When adding approximately 1 virus per cell (MOI 1), we detected luciferase 3 hours following infection. The signal displayed a maximum peak at 5 hours post infection. This suggests the time from entry to peak protein production occurs within 5 hours of infection. Consistent with previous research, kinetics of virus production have been demonstrated to peak between 3.5 to 6.5 hours post-infection when infecting BHKs at MOIs between 5 and 80 [150]. When more virions are added per cell, the luciferase signal is detected earlier during the course of the infection, but the peak luciferase signals were not significantly different. Lower MOIs displayed a steady increase in luciferase signal, but plateau phases between rounds of replication were difficult to observe.

To compare luciferase activity across different cell types, we seeded Veros, HAP1, and HEK293T at the same cell density and infected them with equal volume of rVSV/VSVG (MOI 1 $TCID_{50}$ unit/ Vero cell). Because the HEK293T cells did not withstand washing, the viral inoculum was not removed in this experiment. This change in procedure affected luciferase signals as shown by comparing the Vero MOI 1 data between figure 3.2 a and b and suggest that additional virus continues to enter after 1 hour which enables more luciferase to be produced. In addition, the luciferase substrate is also present for the length of the infection figure 3.2.b, which may further contribute to the higher peak values. Within this experiment, rVSV/VSVG-infected Veros and HAP1 cells displayed similar initial signals and peak times (between 11- and 12-hours post-infection), however, Veros reached a higher peak than HAP1s. Luciferase production in HEK293T cells was

slower than in Veros and HAP1 cells; peak values were similar to those in the HAP1 cell line, but were observed 3 hours later (**figure 3.2.b**).

Kinetics of rVSV/LASVGPC Luciferase Expression

Once we established how quickly we could detect luciferase signal when rVSV was entering using the its native glycoprotein VSV G, we wanted to compare how quickly signals were produced when the rVSV was coated in the LASV GPC. Unlike VSV G which fuses with early endosomal membranes, LASV fusion requires very low pH values found in late endosomes/lysosomes and therefore we predicted luciferase production would both start and peak at later time points than VSV G. To determine signal peak and relative strength, we infected Veros at a MOI of 25, 5, 1, 0.2, and 0.5 (PFU/cell). At a MOI of 25, luciferase expression was evident at 2-hour post-infection and displayed a maximum signal peak at 4 hours, notably slower than VSVG. When decreasing MOIs by 5-fold, luciferase signal and signal peak was detected at later times in comparison to a MOI of 25 (**figure 3.3.a**).

Evaluation of Veros, HAP1, HAP1ΔDAG1, and HEK293T cell lines during rVSV/LASVGPC infection, demonstrated complete overlapping kinetics of luciferase expression during the first 6 hours post-infection (except for HAP1ΔDAG1s). At 8 hours post-infection, Veros reached a higher signal in comparison to HAP1 and HEK293T cells (**figure 3.3.b**). For cells lacking the LASV αDG receptor, HAP1ΔDAG1, we observed near-background luciferase signal for the entire 12 hours. It is known that adding enough virus onto the HAP1ΔDAG1 cells can overcome the entry block [81,146], thus, we increased the viral load by a 100-fold, and could attain similar luciferase signal strength to that of HAP1 cells (**figure 3.3.c**). This observation led us to inquire whether

rVSV/LASVGP is utilizing a different endocytic pathway to enter cells lacking the αDG receptor, because previous research has reported LASV GPC entry occurs in a macropinocytosis-like pathway via αDG [87]. To test this, we infected HAP1 and HAP1ΔDAG1 at a MOI of 1 and 100 respectively, and measured luminescence in the presence of entry inhibitors nystatin, EIPA, dynasore, and chlorpromazine. After normalization, both HAP1 and HAP1ΔDAG1 cells displayed no differences in inhibition pattern (**figure 3.3.d**).

Kinetics of rVSV/EBOVGP Luciferase Expression

Next, we examined rVSV/EBOVGP entry. Like LASV, EBOV entry requires virions to traffic into more mature endosomes before fusion can occur [151]. Infection of Veros with rVSV/EBOVGP at a MOI of 25 (PFU/cell), resulted in a signal peak at 4.5 hours post-infection and at a MOI of 1 (PFU/cell) the signal peaked around 7 hours. With decreasing MOIs (5-fold reduction), luciferase signal peak levels were detected at later times relative to that of MOI of 25 (**figure 3.4.a**).

rVSV/EBOVGP infection comparison between Veros, HAP1, and HEK293T cells, yielded comparably low luciferase activity (**figure 3.4.b top**). Despite the relatively high MOI utilized (25 TCID50 unit/ Vero cell), HAP1 and HEK293T showed only minor signals above baseline levels of luciferase expression (**figure 3.4.b bottom**). While it has been reported that HEK293Ts are not highly susceptible for EBOV entry [125], EBOV entry into HAP1 cells has been widely reported. In fact, the NPC1 receptor was identified by HAP1 cells infected with rVSV/EBOVGP [140].

Attachment factors play a key role in the facilitation of viral entry of EBOV. Since HEK293T cells naturally lack endogenous PS receptors and C-type lectins, we wanted to

evaluate whether luciferase signal could be enhanced by transiently expressing attachment factors. We transfected HEK293Ts with L-SIGN, Axl, Tyro3, and TIM-1-GFP and confirmed protein production by immunoblotting (**figure 3.4.c**). In our results, HEK293T cells transfected with L-SIGN and TIM-1-GFP, reached a higher signal value upon rVSV/EBOVGP infection in comparison to the control group, with signals peaking first when L-SIGN was present. In contrast, HEK293T cells transfected with Axl and Tyro3 remained at baseline level and no significant change was observed (**figure 3.4.d**). Note that HEK293T (control) from figure 3.4.d yielded higher signals than HEK293T from figure 3.3.b, this could be achieved by increasing the seeding density and amount of virus added to amplify the signal.

Comparative analysis of rVSV viruses' kinetics of luciferase expression.

We decided to compare rVSV/VSVG, -EBOVGP, and -LASVGPC directly by overlaying some of the data obtained when Veros were infected at multiple MOIs. VSV mRNA production occurs in a transcription gradient, with the open reading frame (ORF) at the beginning of the genome produced at a higher level than those at the end of the genome [152]. Because the luciferase reporter gene was cloned after the glycoprotein gene for all constructs, we were concerned that the delay observed in rVSV/EBOVGP signal production could be due to the increased length of the EBOV GP (2,031 bases) [101] compared to that of VSV G (1,536 bases) [153] or LASV GP (1,476 bases) [154]. To assess this possibility, we used rVSV/CHIKVE as a control, given that the gene encoding for the envelope (2,961 bases) [147] is twice the length size as the VSV G and LASV GPC and about 1,000 bp longer than EBOV GP gene. Here we found that both rVSV/VSVG and rVSV/CHIKVE signals overlap and were detected an hour earlier than rVSV/LASVGPC

and rVSV/EBOVGP. Furthermore, rVSV/LASVGPC show a faster signal in comparison to rVSV/EBOVGP (**figure 3.5.a-b**). This pattern was consistent across all MOIs (not shown).

In addition to measuring luciferase signals, we assessed viral replication kinetics by performing a multistep replication curve and quantifying viral titers. We infected Veros for 1 hour at a MOI of 0.01 (PFU/cell) and collected the supernatant at time 0. 4, 8, 12, 18, 24 and 48. As expected, we found higher titers in supernatants when cells were infected with rVSV/CHIKVE and rVSV/VSVG. Surprisingly, rVSV/EBOVGP displayed higher titers than rVSV/LASVGPC (**figure 3.5.c**), even though luciferase signals was always higher for rVSV/LASVGPC-infected cells.

Endocytosis mechanism of rVSV viruses.

Since the length of the envelope does not seem to affect how early signal is detected, we decided to evaluate if differences in the luciferase production were a result of viruses utilizing distinct endocytic pathways. Given that macropinocytosis and caveolae uptake occurs at slower rates than clathrin-mediated endocytosis [11,15,19], We infected Veros in the presence of endocytic drug inhibitors nystatin, EIPA, dynasore, and chlorpromazine, and measured luciferase expression over time. The data represents percent of control (DMSO) of the last time-point measured. Surprisingly, we found similar degrees of inhibition across rVSV viruses regardless of the glycoprotein expressed (**figure 3.6**).

Discussion

LHF and EVD are two types of VHF caused by LASV and EBOV, respectively. These diseases are endemic in West Africa and are responsible for significant mortality and economic burden in the region. Both viruses are classified as BSL-4 pathogens, which

greatly limits the number of researchers who can study these viruses. However, the glycoprotein alone is sufficient to study viral entry into host cells and can be incorporated into models appropriate for BSL-2 facilities. We generated rVSV viruses pseudotyped with EBOV and LASV glycoproteins to study entry kinetics using a luciferase reporter gene cloned within the VSV genome and compare how rapidly the different glycoproteins are trafficked within one cell type because the VSV replication machinery was the same for all viruses.

Interestingly, when comparing kinetics of luciferase expression in rVSV/LASVGPC-infected Veros, HAP1, and HEK293T cells, there were no differences within the first 6 hours. Veros lack properly glycosylated αDG –required for efficient LASV GPC binding [79], yet Veros demonstrated higher luciferase production 8 hours post-infection than HEK293T and HAP1 cells (figure 3.3.b). It is difficult to determine if the higher signals detected in Vero cells are due to increased permissiveness, enhanced efficiency machinery or other cellular factors. For example, Vero cells are known to lack an interferon response, so it is capable to produce high viral titers. They are also significantly larger than both HEK293T and HAP1 and may simply have more resources to produce more luciferase than the smaller cells. Both VSV G and LASV GP resulted in higher peak signals in the Vero cells, which may suggest peak values are limited in the other cell lines (figure 3.2 and 3.3.a). Further experiments will need to be performed to determine if the level of reporter gene expression is limited within a given cell irrespective of the glycoprotein used for entry. As expected, rVSV/LASVGPC-infected HAP1ΔDAG1 cells displayed remarkably low luciferase activity compared to infected HAP1 cells (figure 3.3.b), but when infecting HAP1ΔDAG1 at a higher MOI, the signals could be roughly

matched (figure 3.3.c). This suggests rVSV/LASVGPC is approximately 100-fold less efficient entering cells lacking αDG. Several PS receptors have been shown to mediate LASV entry in the absence of the functional receptor [83-85]. Since HAP1 cells do not to express Axl or TIMs (data available from v19.3 proteinatlas.org), and because Mer does not play a significant role during LASV infection [83], rVSV/LASVGPC is likely able to enter HAP1ΔDAG1 via Tyro3 and/or heparan sulfate [81,83]. Further testing is needed to confirm this observation. In addition, the possibility of other unidentified receptors playing a role during LASV entry cannot be ignored. Regardless of the presence of αDG, rVSV/LASVGPC seems to be internalized via the same endocytic pathways in both HAP1 and HAP1ΔDAG1 cells. We utilized inhibitors specific to macropinocytosis (EIPA), clathrin-(chlorpromazine), and caveola-mediated endocytosis (nystatin) and each endocytosis blocker exhibited the same pattern of inhibition across HAP1 and HAP1ΔDAG1 cells (figure 3.3.d), suggesting that the uptake pathway is not dystroglycan-dependent. This conflicts with previous research that used different cell lines and LASV models [86,87]. Nonetheless, the fact that particle morphology greatly impacts the mode of entry cannot be overlooked as seen during VSV and influenza virus [39,155,156]. Overall, this assay allows comparison between cell line knockouts and is sensitive enough to detect luciferase expression when the efficiency difference is roughly 100-fold.

During rVSV/EBOVGP infection, HAP1 and HEK293Ts exhibited exceptionally low luciferase activity compared to Veros, even when infecting cells at a high MOI (figure 3.4.b). We were surprised to find that HAP1 cells were almost refractory to rVSV/EBOVGP infection despite naturally expressing Tyro3 and Mer, which were found to mediate EBOV GP entry by other groups [126,128]. Because luciferase expression of

HAP1 and HEK293Ts are similar, it suggests that Tyro3 and Mer may not play an important role during rVSV/EBOVGP infection [126,157]. This was confirmed by transiently expressing Tyro3 in HEK293Ts, which resulted in no enhancement of luciferase activity when compared to GFP-transfected HEK293Ts (control). Similar studies are needed to evaluate the significance of Mer. Transfection of Axl did not enhance luciferase expression in HEK293Ts either, also conflicting with previous research [127-129]. It is worth noting that many lab groups utilize different models, including authentic EBOV, to study entry however, the details about differences and similarities about experimental design will not be discussed here. L-SIGN and TIM-1 in HEK293T enhanced entry kinetics of rVSV/EBOVGP (figure 3.4.d), consistent with previous research [125,128,157,158]. All proteins were confirmed to be expressed in HEK293T by immunoblotting (figure 3.4.c). Our data also suggest that L-SIGN enables more rapid uptake of EBOVGP than TIM1. While previous work has suggested various proteins increase entry, here we can demonstrate some entry enhancement factors increase how quickly the virion is trafficked within the cell to the fusion compartment. Overall, this assay allows comparing kinetics of luciferase expression in transfected cells expressing attachment factors.

As expected, with increasing MOIs we found that luciferase activity and peak times were detected earlier than at lower MOIs because the signal is amplified (figure 3.2.a, 3.3.a, 3.4.a). In the case of rVSV/VSVG infection at a MOI of 25, moderately high luciferase activity was observed one-hour post-infection and was three orders of magnitude higher than rVSV/LASVGPC and rVSV/EBOVGP (figure 3.5.a), a trend that remained consistent across MOIs (25-0.04). Since permissiveness is controlled by cell line and replication machinery, and only the expressed glycoprotein is different in the vector, we can attribute

the delay of luciferase expression to entry differences. We discarded the possibility that the signal delay could result from the increased envelope glycoprotein length, which is transcribed before the reporter gene, because rVSV/CHIKVE kinetics overlapped with rVSV/VSVG, despite CHIKV E gene being approximately as twice as long than the VSV G gene [153,159] and longer than the EBOV GP gene [101]. These luciferase signal differences could be due to binding, internalization, and/or fusion delays. Therefore, both VSV G [42] and CHIKV E [160] which fuse with the early endosomes, produced luciferase signals at a faster rate, than EBOVGP and LASVGPC which have more complicated entry processes. Although LASV entry requires exposure to very acidic pH for triggering in the late endosome/lysosome [161], it was able to induce signals faster than EBOV GP. EBOV GP entry must undergo a protease cleavage event in addition to trafficking to endolysosome where interaction with NPC1 can induce fusion [162]. The additional proteolysis steps appear to slow the EBOV entry process, requiring more time before fusion pore formation.

Conventional replication curves performed on Veros demonstrate that rVSV/VSVG and rVSV/CHIKVE produce higher viral titers faster than rVSV/EBOVGP and rVSV/LASVGPC (figure 3.5.c). Surprisingly, rVSV/EBOVGP infection results in higher titers than rVSV/LASVGP infection even though luciferase expression is always delayed and reduced. This may suggest the EBOVGP is able to be incorporated onto the rVSV particle more efficiently than the LASVGPC.

Since endocytic pathways internalize cargo at different rates, we decided to investigate whether luciferase expression delays were due to different endocytic pathways being triggered by the different envelopes, we utilized the previously mentioned entry blockers of endocytosis in Vero cells, and found no significant differences in the pattern of

inhibition each drug had across the different viruses (figure 3.6). As discussed earlier, virion morphology impacts the endocytic pathway and seems to be irrespective of the glycoprotein being expressed. Nonetheless, these results lead us to believe that the internalization process happens at the same rate upon triggering endocytosis. However, it does not mean the proportion of viruses entering the cell is the equal because binding and interactions with other receptors could be different from virus to virus. However, this hypothesis must be subjected for testing.

In conclusion, we can use rVSV viruses to study entry kinetics of LASV and EBOV even though this assay is not detecting fusion events specifically but rather replication efficiency. When comparing multiple cell lines, additional experiments will be needed to determine permissiveness, however, we can still compare general patterns with a control, and compare within the same cell line to correlate the data to entry. A limitation of this model is that particle morphology of VSV is radically distinct from authentic LASV and EBOV and therefore, when determining endocytic pathways, this model is not ideal.

A new split luciferase, NanoBiT®, has come out from Promega, and viral fusion assays with this component would require an 11-amino-acid peptide to be inserted into a viral structural protein. Once delivered into the cell, would interact with the larger piece of luciferase, and produce a signal. We should be able to use this system to develop an assay to detect fusion as we initially intended because the split luciferase would not have the background signal associated with the viral particles that we detected having the entire luciferase protein in the virus. Once this virus is recovered it will be interesting to compare the signals between the viruses described here and further determine the specific time points that fusion versus mRNA and protein expression occur in VSV replication.

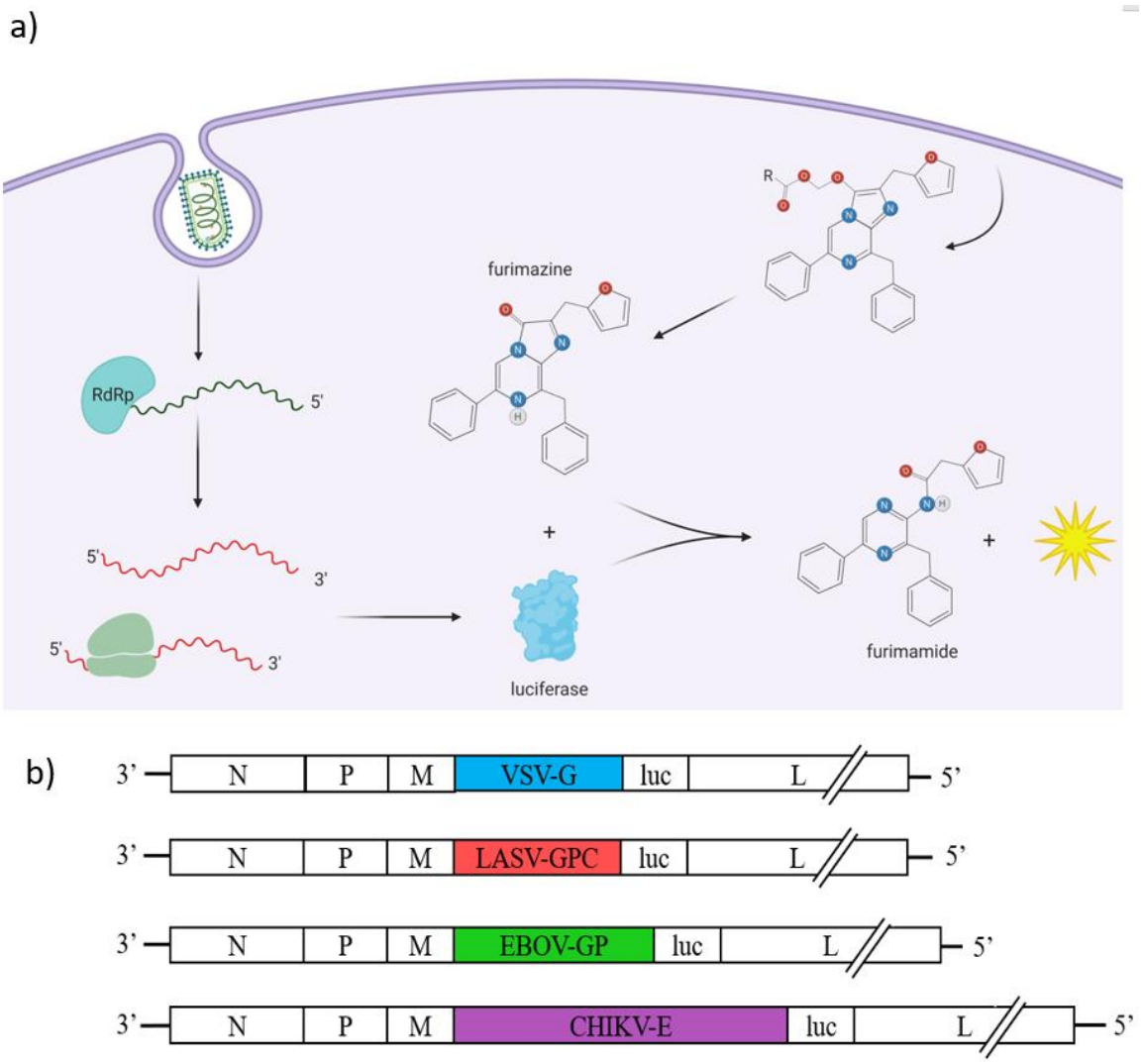

Figure 3.1. Schematic of rVSV viruses and luciferase reaction. a) Upon viral endocytosis and genome release into the cytoplasm, the viral RNA-dependent-RNA polymerase produces mRNA for all the ORFs in the genome, including luciferase. The substrate diffuses through the plasma membrane and must be hydrolyzed by cellular esterases and only then, luciferase is able to oxidize furimazine and generate light. **b)** The Nanoluciferase gene is 636 base pairs long and was cloned within the envelope and polymerase genes. We have produced four rVSV-Nluc viruses expressing the native glycoprotein (VSV) and foreign glycoproteins (LASV, EBOV, and CHIKV envelopes). (back).

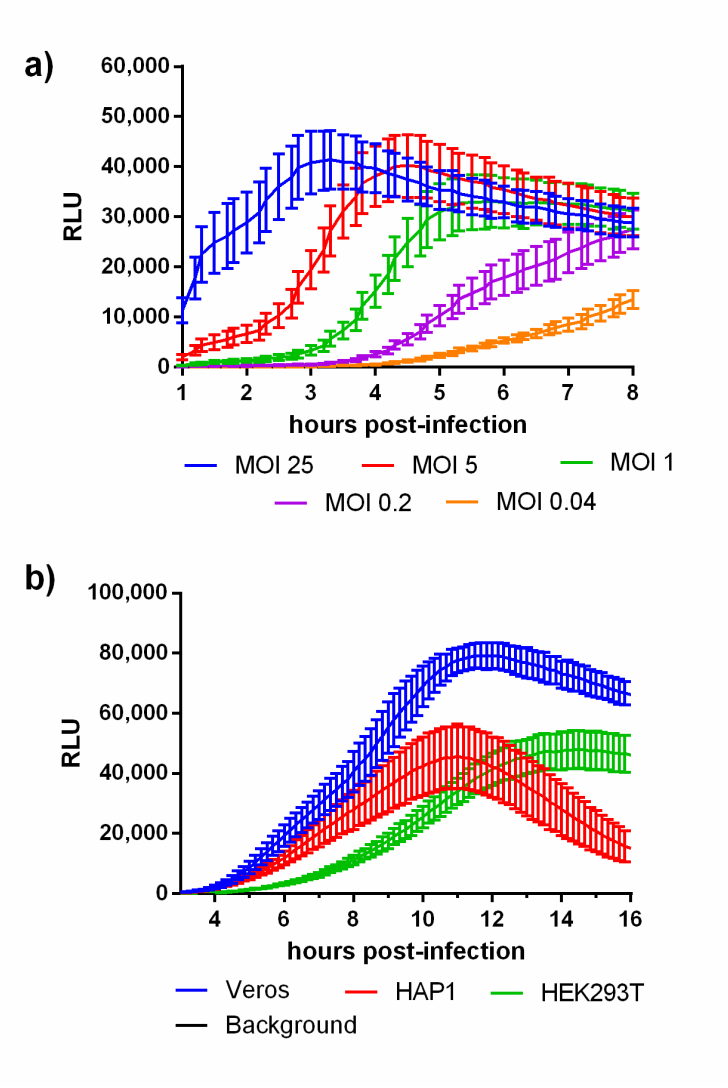

Figure 3.2. Kinetics of rVSV/VSVG luciferase expression. a) Vero cells were seeded at a density of $2.0x10^4$ cells/well. Forty-eight hours later, substrate was preincubated with cells for 1 hour, then infected at multiple MOIs (PFU/cell) for an hour. Media was replaced with phenol red-free media containing HEPES and luminescence was measured every 10 minutes. This Figure is the result of 3 independent trials performed in duplicates. **b)** Cells were seeded at a density of $1.50x10^4$ cells/well, twenty-four hours later, cells were infected in the presence of substrate at a MOI of 1 ($TCID_{50}$ unit/Vero cell). Unlike part a, Luminescence was measured in the presence of substrate and initial inoculum. This figure is the result of three independent trials performed in triplicates (back).

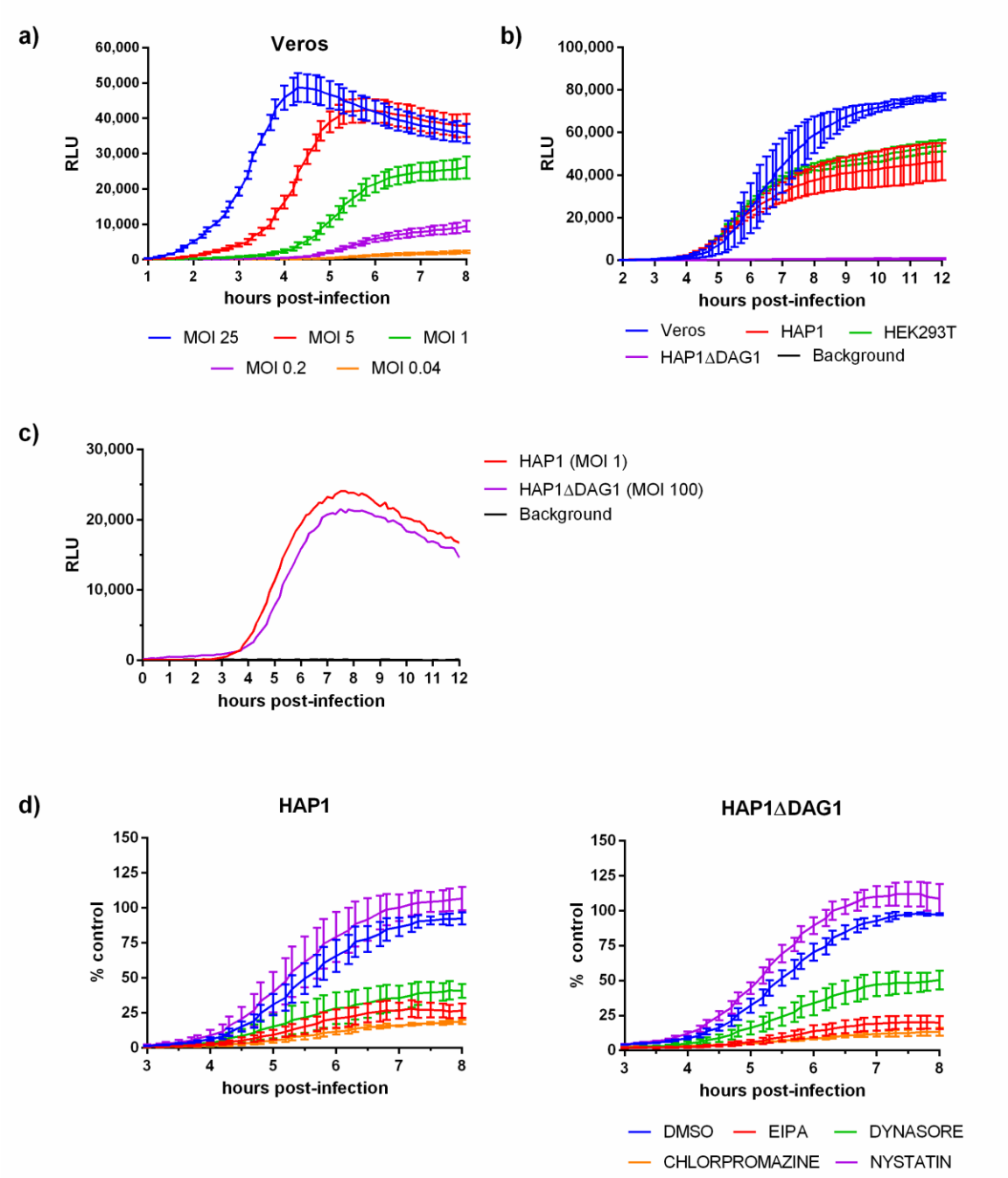

Figure 3.3. Kinetics of rVSV/LASVGPC luciferase expression. a) Vero cells were seeded at a density of $2.0x10^4$ cells/well. Forty-eight hours later, substrate was preincubated with cells for 1 hour, then infected at multiple MOIs (PFU/cell) for an hour. Media was replaced with phenol red-free media containing HEPES and luminescence was measured every 10 minutes. This figure is the result of 5 independent trials performed in duplicates. **b)** Cells were seeded at a density of $1.50x10^4$ cells/well, twenty-four hours later, cells were infected in the presence of substrate at a MOI of 1 ($TCID_{50}$ unit/Vero cell). Unlike part a, luminescence was measured in the presence of substrate and initial inoculum. This figure is the result of three independent trials performed in triplicates. **c)** HAP1 and HAP1ΔDAG1

were seeded at the same density and infected at a MOI of 1 and 100, respectively. Cells were infected as described in part b. This figure is the result of one trial performed in duplicate. **d)** HAP1 and HAP1ΔDAG1 were pre-incubated with DMSO (control), EIPA (50 µM), dynasore (6.25 µM), nystatin (30 µg/ml), or chlorpromazine (0.625 µg/ml) for 30 minutes prior infection, then proceeded as described in part b. Luminescence was normalized to the highest value from the control and results are shown as percentage. Concentrations were chosen based on HAP1 viability with a mean equal or greater than 80% with the Promega CellTiter Glo Kit. This figure is the result of three independent trials performed in triplicates (back).

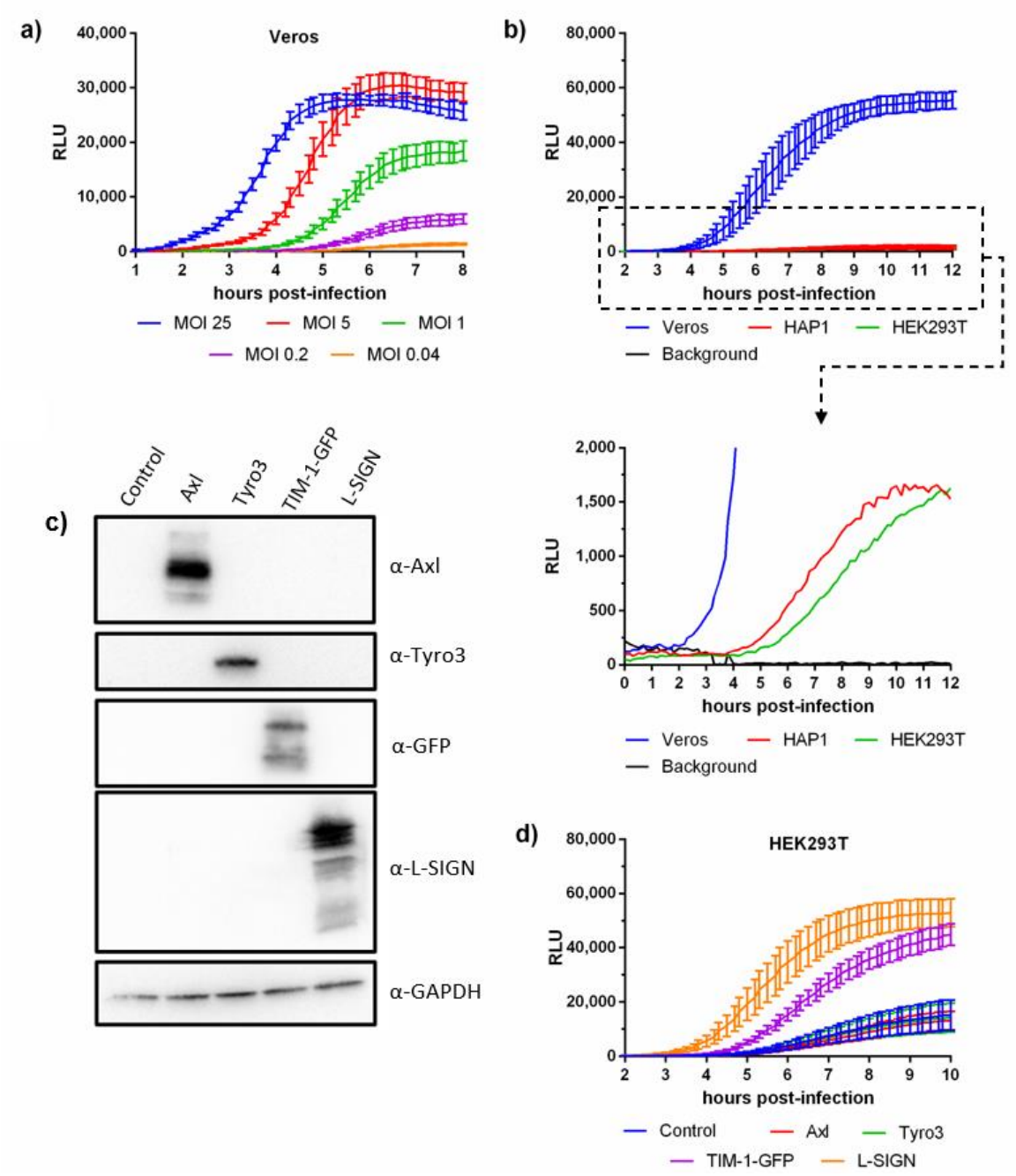

Figure 3.4. Kinetics of rVSV/EBOVGP luciferase expression. a) Vero cells were seeded at a density of $2.0x10^4$ cells/well. Forty-eight hours later, substrate was preincubated with cells for 1 hour, then infected at multiple MOIs (pfu/cell) for an hour. Media was replaced with phenol red-free media containing HEPES and luminescence was measured every 10 minutes. This figure is the result of 5 independent trials performed in duplicates. **b)** Cells were seeded at a density of $1.5x10^4$ cells/well, twenty-four hours later, cells were infected in the presence of substrate at a MOI of 25 ($TCID_{50}$ unit/Vero cell). Unlike part a, Luminescence was measured in the presence of substrate and initial inoculum. This figure is the result of three independent trials performed in triplicates. **c)** Cells were seeded in 6-

well plate and transfected with 2 µg of plasmid expressing attachment factors or GFP (control), 4 hours post-transfection, media was replaced. Half of the cells were collected 24 hours post-transfection by treating with trypsin and pelleting them. Pellet was resuspended in 100 µl of PBS and lysed with 100 µl of lysis buffer; and spin-cleared of insoluble material. Then, 160 µl was denatured and 30 µl was loaded per lane. Membrane was blocked for 2 hours at room temperature with 10% milk in PBST. Primary antibody was incubated for 3 hours and secondary antibody for 45 minutes at room temperature. GFP only (lane 1), Axl (lane 2), Tyro3 (lane 3), TIM1-GFP (lane 4), and L-SIGN (lane 5). GAPDH serves as a loading control. **d)** HEK293T cells were seeded in 96-well plates at a density of $3.0x10^4$ cells/well, transfected next day with 10 ng of DNA per well. Two hours post-transfection, half of the media was replaced. Twenty-four-hour post-transfection, cells were infected as described in part c. This figure is the result of four independent trials in triplicates (back).

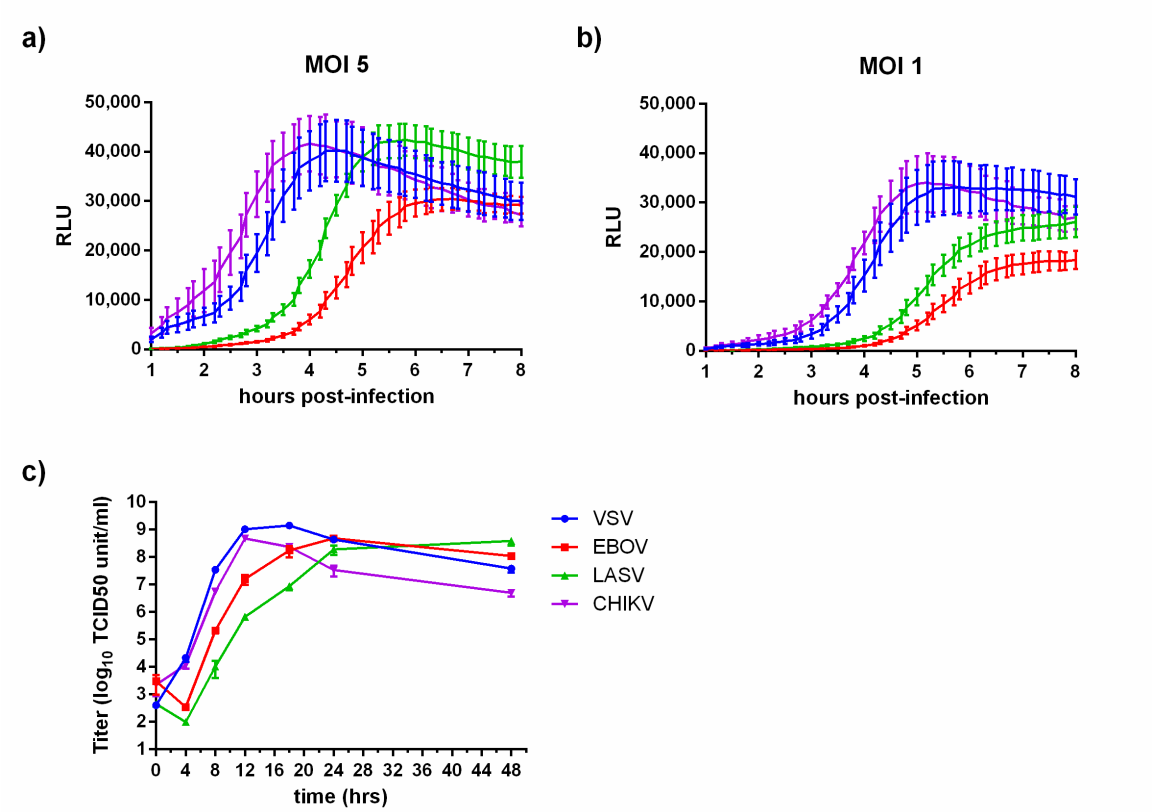

Figure 3.5. Comparative analysis of rVSV viruses' kinetics of luciferase expression. a) and **b)** represent the data from figure 3.2.a, 3.3.a, and 3.4.a re-graphed. r/VSVCHIKVE experiments were performed in the same manner (three independent times in duplicates). The kinetics of luciferase expression of rVSV/VSVG and -CHIKVE closely overlap and are faster than -LASVGPC, which is faster than -EBOVGP, a trend that was consistent across all MOIs. **c).** Multi-step replication curve. EBOV and LASV curves are the result of 7 independent trials, VSV of 4 independent trials, and CHIKV of 2 independent trials (back).

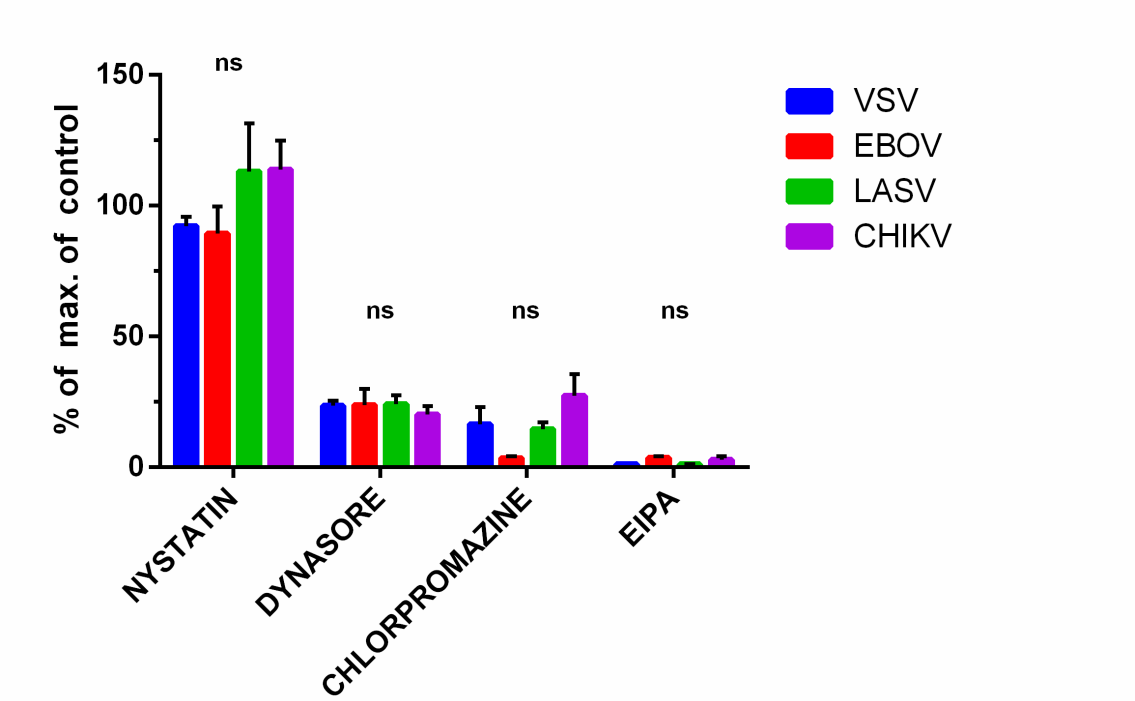

Figure 3.6. Endocytosis mechanism of rVSV viruses. $2.0x10^4$ cells/well were seeded in 96-well plate. Forty-eight hours later, media was replaced with phenol red-free media containing entry inhibitors nystatin (30 µg/ml), EIPA (100 µM), dynasore (50 µM), chlorpromazine (0.625 µg/ml) and pre-incubated for 30 minutes prior infection. Cells were infected with rVSV viruses at MOI of 1 ($TCID_{50}$ unit/cell) and luminescence was measured every 10 minutes in the presence of drug, inoculum, and substrate for 8 hours. Luminescence was normalized to control (DMSO) and shown as percentage. Concentrations were chosen based on Vero viability with a mean equal or greater than 80% with the Promega CellTiter-Glo kit. The figure displays the percentages of the last time point only, performed three independent trials in triplicates. Statistical analysis: Two-way ANOVA multiple comparison Tukey's Test was done in GraphPad Prism 6 (go to Discussion).

REFERENCES

1. Zapata, J.C.; Cox, D.; Salvato, M.S. The role of platelets in the pathogenesis of viral hemorrhagic fevers. *PLoS Negl Trop Dis* **2014**, *8*, e2858, doi:10.1371/journal.pntd.0002858.

2. Cossart, P.; Helenius, A. Endocytosis of viruses and bacteria. *Cold Spring Harb Perspect Biol* **2014**, *6*, doi:10.1101/cshperspect.a016972.

3. Mercer, J.; Schelhaas, M.; Helenius, A. Virus entry by endocytosis. *Annu Rev Biochem* **2010**, *79*, 803-833, doi:10.1146/annurev-biochem-060208-104626.

4. Hu, Y.B.; Dammer, E.B.; Ren, R.J.; Wang, G. The endosomal-lysosomal system: from acidification and cargo sorting to neurodegeneration. *Transl Neurodegener* **2015**, *4*, 18, doi:10.1186/s40035-015-0041-1.

5. Huotari, J.; Helenius, A. Endosome maturation. *EMBO J* **2011**, *30*, 3481-3500, doi:10.1038/emboj.2011.286.

6. Haigler, H.T.; McKanna, J.A.; Cohen, S. Rapid stimulation of pinocytosis in human carcinoma cells A-431 by epidermal growth factor. *J Cell Biol* **1979**, *83*, 82-90, doi:10.1083/jcb.83.1.82.

7. Racoosin, E.L.; Swanson, J.A. Macrophage colony-stimulating factor (rM-CSF) stimulates pinocytosis in bone marrow-derived macrophages. *J Exp Med* **1989**, *170*, 1635-1648, doi:10.1084/jem.170.5.1635.

8. Swanson, J.A. Phorbol esters stimulate macropinocytosis and solute flow through macrophages. *J Cell Sci* **1989**, *94*, 135-142.

9. Swanson, J.A.; Watts, C. Macropinocytosis. *Trends Cell Biol* **1995**, *5*, 424-428, doi:10.1016/s0962-8924(00)89101-1.

10. Norbury, C.C.; Chambers, B.J.; Prescott, A.R.; Ljunggren, H.G.; Watts, C. Constitutive macropinocytosis allows TAP-dependent major histocompatibility complex class I presentation of exogenous soluble antigen by bone marrow-derived dendritic cells. *Eur J Immunol* **1997**, *27*, 280-288, doi:10.1002/eji.1830270141.

11. Kerr, M.C.; Teasdale, R.D. Defining macropinocytosis. *Traffic* **2009**, *10*, 364-371, doi:10.1111/j.1600-0854.2009.00878.x.

12. Koivusalo, M.; Welch, C.; Hayashi, H.; Scott, C.C.; Kim, M.; Alexander, T.; Touret, N.; Hahn, K.M.; Grinstein, S. Amiloride inhibits macropinocytosis by lowering submembranous pH and preventing Rac1 and Cdc42 signaling. *J Cell Biol* **2010**, *188*, 547-563, doi:10.1083/jcb.200908086.

13. Bitsikas, V.; Correa, I.R., Jr.; Nichols, B.J. Clathrin-independent pathways do not contribute significantly to endocytic flux. *Elife* **2014**, *3*, e03970, doi:10.7554/eLife.03970.

14. Liu, A.P.; Aguet, F.; Danuser, G.; Schmid, S.L. Local clustering of transferrin receptors promotes clathrin-coated pit initiation. *J Cell Biol* **2010**, *191*, 1381-1393, doi:10.1083/jcb.201008117.

15. Kaksonen, M.; Roux, A. Mechanisms of clathrin-mediated endocytosis. *Nat Rev Mol Cell Biol* **2018**, *19*, 313-326, doi:10.1038/nrm.2017.132.

16. Wang, L.H.; Rothberg, K.G.; Anderson, R.G. Mis-assembly of clathrin lattices on endosomes reveals a regulatory switch for coated pit formation. *J Cell Biol* **1993**, *123*, 1107-1117, doi:10.1083/jcb.123.5.1107.

17. Parton, R.G. Caveolae: Structure, Function, and Relationship to Disease. *Annu Rev Cell Dev Biol* **2018**, *34*, 111-136, doi:10.1146/annurev-cellbio-100617-062737.

18. Kirkham, M.; Fujita, A.; Chadda, R.; Nixon, S.J.; Kurzchalia, T.V.; Sharma, D.K.; Pagano, R.E.; Hancock, J.F.; Mayor, S.; Parton, R.G. Ultrastructural identification of uncoated caveolin-independent early endocytic vehicles. *J Cell Biol* **2005**, *168*, 465-476, doi:10.1083/jcb.200407078.

19. Shvets, E.; Bitsikas, V.; Howard, G.; Hansen, C.G.; Nichols, B.J. Dynamic caveolae exclude bulk membrane proteins and are required for sorting of excess glycosphingolipids. *Nat Commun* **2015**, *6*, 6867, doi:10.1038/ncomms7867.

20. Le Lay, S.; Hajduch, E.; Lindsay, M.R.; Le Liepvre, X.; Thiele, C.; Ferre, P.; Parton, R.G.; Kurzchalia, T.; Simons, K.; Dugail, I. Cholesterol-induced caveolin targeting to lipid droplets in adipocytes: a role for caveolar endocytosis. *Traffic* **2006**, *7*, 549-561, doi:10.1111/j.1600-0854.2006.00406.x.

21. Payne, C.K.; Jones, S.A.; Chen, C.; Zhuang, X. Internalization and trafficking of cell surface proteoglycans and proteoglycan-binding ligands. *Traffic* **2007**, *8*, 389-401, doi:10.1111/j.1600-0854.2007.00540.x.

22. Macia, E.; Ehrlich, M.; Massol, R.; Boucrot, E.; Brunner, C.; Kirchhausen, T. Dynasore, a cell-permeable inhibitor of dynamin. *Dev Cell* **2006**, *10*, 839-850, doi:10.1016/j.devcel.2006.04.002.

23. Nabi, I.R.; Le, P.U. Caveolae/raft-dependent endocytosis. *J Cell Biol* **2003**, *161*, 673-677, doi:10.1083/jcb.200302028.

24. LeNeveu, D.M.; Rand, R.P.; Parsegian, V.A. Measurement of forces between lecithin bilayers. *Nature* **1976**, *259*, 601-603, doi:10.1038/259601a0.

25. Chernomordik, L.V.; Kozlov, M.M. Membrane hemifusion: crossing a chasm in two leaps. *Cell* **2005**, *123*, 375-382, doi:10.1016/j.cell.2005.10.015.

26. Harrison, S.C. Viral membrane fusion. *Virology* **2015**, *479-480*, 498-507, doi:10.1016/j.virol.2015.03.043.

27. Plemper, R.K. Cell entry of enveloped viruses. *Curr Opin Virol* **2011**, *1*, 92-100, doi:10.1016/j.coviro.2011.06.002.

28. White, J.M.; Whittaker, G.R. Fusion of Enveloped Viruses in Endosomes. *Traffic* **2016**, *17*, 593-614, doi:10.1111/tra.12389.

29. Gaudin, Y.; Tuffereau, C.; Segretain, D.; Knossow, M.; Flamand, A. Reversible conformational changes and fusion activity of rabies virus glycoprotein. *J Virol* **1991**, *65*, 4853-4859.

30. Zhou, J.; Blissard, G.W. Mapping the conformational epitope of a neutralizing antibody (AcV1) directed against the AcMNPV GP64 protein. *Virology* **2006**, *352*, 427-437, doi:10.1016/j.virol.2006.04.041.

31. United States Department of Agriculture. Foot and Mouth Disease. Availabe online: https://www.aphis.usda.gov/aphis/ourfocus/animalhealth/animal-disease-information/fmd (accessed on 22 June 2020).

32. Rozo-Lopez, P.; Drolet, B.S.; Londono-Renteria, B. Vesicular Stomatitis Virus Transmission: A Comparison of Incriminated Vectors. *Insects* **2018**, *9*, doi:10.3390/insects9040190.

33. United States Department of Agriculture. Vesicular stomatitis. Availabe online: https://www.aphis.usda.gov/aphis/ourfocus/animalhealth/animal-disease-information/cattle-disease-information/vesicular-stomatitis-info (accessed on 22 June 2020).

34. Quiroz, E.; Moreno, N.; Peralta, P.H.; Tesh, R.B. A human case of encephalitis associated with vesicular stomatitis virus (Indiana serotype) infection. *Am J Trop Med Hyg* **1988**, *39*, 312-314, doi:10.4269/ajtmh.1988.39.312.

35. McCombs, R.M.; Benyesh-Melnick, M.; Brunschwig, J.P. Biophysical Studies of Vesicular Stomatitis Virus. *J Bacteriol* **1996**, *91*.

36. Roche, S.; Albertini, A.A.; Lepault, J.; Bressanelli, S.; Gaudin, Y. Structures of vesicular stomatitis virus glycoprotein: membrane fusion revisited. *Cell Mol Life Sci* **2008**, *65*, 1716-1728, doi:10.1007/s00018-008-7534-3.

37. Amirache, F.; Levy, C.; Costa, C.; Mangeot, P.E.; Torbett, B.E.; Wang, C.X.; Negre, D.; Cosset, F.L.; Verhoeyen, E. Mystery solved: VSV-G-LVs do not allow efficient gene transfer into unstimulated T cells, B cells, and HSCs because they lack the LDL receptor. *Blood* **2014**, *123*, 1422-1424, doi:10.1182/blood-2013-11-540641.

38. Finkelshtein, D.; Werman, A.; Novick, D.; Barak, S.; Rubinstein, M. LDL receptor and its family members serve as the cellular receptors for vesicular stomatitis virus. *Proc Natl Acad Sci U S A* **2013**, *110*, 7306-7311, doi:10.1073/pnas.1214441110.

39. Cureton, D.K.; Massol, R.H.; Whelan, S.P.; Kirchhausen, T. The length of vesicular stomatitis virus particles dictates a need for actin assembly during clathrin-dependent endocytosis. *PLoS Pathog* **2010**, *6*, e1001127, doi:10.1371/journal.ppat.1001127.

40. Cureton, D.K.; Massol, R.H.; Saffarian, S.; Kirchhausen, T.L.; Whelan, S.P. Vesicular stomatitis virus enters cells through vesicles incompletely coated with clathrin that depend upon actin for internalization. *PLoS Pathog* **2009**, *5*, e1000394, doi:10.1371/journal.ppat.1000394.

41. Sun, X.; Yau, V.K.; Briggs, B.J.; Whittaker, G.R. Role of clathrin-mediated endocytosis during vesicular stomatitis virus entry into host cells. *Virology* **2005**, *338*, 53-60, doi:10.1016/j.virol.2005.05.006.

42. Johannsdottir, H.K.; Mancini, R.; Kartenbeck, J.; Amato, L.; Helenius, A. Host cell factors and functions involved in vesicular stomatitis virus entry. *J Virol* **2009**, *83*, 440-453, doi:10.1128/JVI.01864-08.

43. Superti, F.; Seganti, L.; Ruggeri, F.M.; Tinari, A.; Donelli, G.; Orsi, N. Entry pathway of vesicular stomatitis virus into different host cells. *J Gen Virol* **1987**, *68 (Pt 2)*, 387-399, doi:10.1099/0022-1317-68-2-387.

44. Yao, Y.; Ghosh, K.; Epand, R.F.; Epand, R.M.; Ghosh, H.P. Membrane fusion activity of vesicular stomatitis virus glycoprotein G is induced by low pH but not by heat or denaturant. *Virology* **2003**, *310*, 319-332, doi:10.1016/s0042-6822(03)00146-6.

45. Whelan, S.P.; Ball, L.A.; Barr, J.N.; Wertz, G.T. Efficient recovery of infectious vesicular stomatitis virus entirely from cDNA clones. *Proc Natl Acad Sci U S A* **1995**, *92*, 8388-8392, doi:10.1073/pnas.92.18.8388.

46. Lawson, N.D.; Stillman, E.A.; Whitt, M.A.; Rose, J.K. Recombinant vesicular stomatitis viruses from DNA. *Proc Natl Acad Sci U S A* **1995**, *92*, 4477-4481, doi:10.1073/pnas.92.10.4477.

47. Takada, A.; Robison, C.; Goto, H.; Sanchez, A.; Murti, K.G.; Whitt, M.A.; Kawaoka, Y. A system for functional analysis of Ebola virus glycoprotein. *Proc Natl Acad Sci U S A* **1997**, *94*, 14764-14769, doi:10.1073/pnas.94.26.14764.

48. Tani, H.; Morikawa, S.; Matsuura, Y. Development and Applications of VSV Vectors Based on Cell Tropism. *Front Microbiol* **2011**, *2*, 272, doi:10.3389/fmicb.2011.00272.

49. Johnson, K.M.; Vogel, J.E.; Peralta, P.H. Clinical and serological response to laboratory-acquired human infection by Indiana type vesicular stomatitis virus (VSV). *Am J Trop Med Hyg* **1966**, *15*, 244-246, doi:10.4269/ajtmh.1966.15.244.

50. Monath, T.P.; Newhouse, V.F.; Kemp, G.E.; Setzer, H.W.; Cacciapuoti, A. Lassa virus isolation from Mastomys natalensis rodents during an epidemic in Sierra Leone. *Science* **1974**, *185*, 263-265, doi:10.1126/science.185.4147.263.

51. Olayemi, A.; Cadar, D.; Magassouba, N.; Obadare, A.; Kourouma, F.; Oyeyiola, A.; Fasogbon, S.; Igbokwe, J.; Rieger, T.; Bockholt, S., et al. New Hosts of The Lassa Virus. *Sci Rep* **2016**, *6*, 25280, doi:10.1038/srep25280.

52. Fichet-Calvet, E.; Rogers, D.J. Risk maps of Lassa fever in West Africa. *PLoS Negl Trop Dis* **2009**, *3*, e388, doi:10.1371/journal.pntd.0000388.

53. Frame, J.D.; Baldwin, J.M., Jr.; Gocke, D.J.; Troup, J.M. Lassa fever, a new virus disease of man from West Africa. I. Clinical description and pathological findings. *Am J Trop Med Hyg* **1970**, *19*, 670-676, doi:10.4269/ajtmh.1970.19.670.

54. Gunther, S.; Lenz, O. Lassa virus. *Crit Rev Clin Lab Sci* **2004**, *41*, 339-390, doi:10.1080/10408360490497456.

55. Center for Disease Control and Prevention. Lassa Fever. Availabe online: https://www.cdc.gov/vhf/lassa/index.html (accessed on 03 June 2020).

56. World Health Organization. Lassa fever. Availabe online: https://www.who.int/news-room/fact-sheets/detail/lassa-fever (accessed on 03 June 2020).

57. McCormick, J.B.; King, I.J.; Webb, P.A.; Scribner, C.L.; Craven, R.B.; Johnson, K.M.; Elliott, L.H.; Belmont-Williams, R. Lassa fever. Effective therapy with ribavirin. *N Engl J Med* **1986**, *314*, 20-26, doi:10.1056/NEJM198601023140104.

58. Ogbu, O.; Ajuluchukwu, E.; Uneke, C.J. Lassa fever in West African sub-region: an overview. *J Vector Borne Dis* **2007**, *44*, 1-11.

59. Murphy, F.A.; Webb, P.A.; Johnson, K.M.; Whitfield, S.G.; Chappell, W.A. Arenoviruses in Vero cells: ultrastructural studies. *J Virol* **1970**, *6*, 507-518.

60. Lukashevich, I.S.; Stelmakh, T.A.; Golubev, V.P.; Stchesljenok, E.P.; Lemeshko, N.N. Ribonucleic acids of Machupo and Lassa viruses. *Arch Virol* **1984**, *79*, 189-203, doi:10.1007/BF01310811.

61. Harnish, D.G.; Dimock, K.; Bishop, D.H.; Rawls, W.E. Gene mapping in Pichinde virus: assignment of viral polypeptides to genomic L and S RNAs. *J Virol* **1983**, *46*, 638-641.

62. Salvato, M.S.; Schweighofer, K.J.; Burns, J.; Shimomaye, E.M. Biochemical and Immunological Evidence That the 11-Kda Zinc-Binding Protein of Lymphocytic Choriomeningitis Virus Is a Structural Component of the Virus. *Virus Research* **1992**, *22*, 185-198, doi:Doi 10.1016/0168-1702(92)90050-J.

63. Vezza, A.C.; Cash, P.; Jahrling, P.; Eddy, G.; Bishop, D.H.L. Arenavirus recombination: The formation of recombinants between prototype pichinde and pichinde munchique viruses and evidence that arenavirus S RNA codes for N polypeptide. *Virology* **1980**, *106*, 250-260, doi:10.1016/0042-6822(80)90248-2.

64. Auperin, D.D.; Romanowski, V.; Galinski, M.; Bishop, D.H. Sequencing studies of pichinde arenavirus S RNA indicate a novel coding strategy, an ambisense viral S RNA. *Journal of Virology* **1984**, *52*, 897-904.

65. Lenz, O.; ter Meulen, J.; Klenk, H.D.; Seidah, N.G.; Garten, W. The Lassa virus glycoprotein precursor GP-C is proteolytically processed by subtilase SKI-1/S1P. *Proc Natl Acad Sci U S A* **2001**, *98*, 12701-12705, doi:10.1073/pnas.221447598.

66. Burri, D.J.; Pasqual, G.; Rochat, C.; Seidah, N.G.; Pasquato, A.; Kunz, S. Molecular characterization of the processing of arenavirus envelope glycoprotein precursors by subtilisin kexin isozyme-1/site-1 protease. *J Virol* **2012**, *86*, 4935-4946, doi:10.1128/JVI.00024-12.

67. Kunz, S.; Edelmann, K.H.; de la Torre, J.-C.; Gorney, R.; Oldstone, M.B.A. Mechanisms for lymphocytic choriomeningitis virus glycoprotein cleavage, transport, and incorporation into virions. *Virology* **2003**, *314*, 168-178, doi:10.1016/s0042-6822(03)00421-5.

68. Schlie, K.; Maisa, A.; Lennartz, F.; Stroher, U.; Garten, W.; Strecker, T. Characterization of Lassa virus glycoprotein oligomerization and influence of cholesterol on virus replication. *J Virol* **2010**, *84*, 983-992, doi:10.1128/JVI.02039-09.

69. Sommerstein, R.; Flatz, L.; Remy, M.M.; Malinge, P.; Magistrelli, G.; Fischer, N.; Sahin, M.; Bergthaler, A.; Igonet, S.; Ter Meulen, J., et al. Arenavirus Glycan Shield Promotes Neutralizing Antibody Evasion and Protracted Infection. *PLoS Pathog* **2015**, *11*, e1005276, doi:10.1371/journal.ppat.1005276.

70. Eichler, R.; Lenz, O.; Garten, W.; Strecker, T. The role of single N-glycans in proteolytic processing and cell surface transport of the Lassa virus glycoprotein GP-C. *Virol J* **2006**, *3*, 41, doi:10.1186/1743-422X-3-41.

71. Eichler, R.; Lenz, O.; Strecker, T.; Garten, W. Signal peptide of Lassa virus glycoprotein GP-C exhibits an unusual length. *FEBS Letters* **2003**, *538*, 203-206, doi:10.1016/s0014-5793(03)00160-1.

72. Eichler, R.; Lenz, O.; Strecker, T.; Eickmann, M.; Klenk, H.D.; Garten, W. Identification of Lassa virus glycoprotein signal peptide as a trans-acting maturation factor. *EMBO reports* **2003**, *4*, 1084-1088, doi:10.1038/sj.embor.7400002.

73. Bederka, L.H.; Bonhomme, C.J.; Ling, E.L.; Buchmeier, M.J. Arenavirus stable signal peptide is the keystone subunit for glycoprotein complex organization. *mBio* **2014**, *5*, e02063, doi:10.1128/mBio.02063-14.

74. Messina, E.L.; York, J.; Nunberg, J.H. Dissection of the role of the stable signal peptide of the arenavirus envelope glycoprotein in membrane fusion. *J Virol* **2012**, *86*, 6138-6145, doi:10.1128/JVI.07241-11.

75. Saunders, A.A.; Ting, J.P.; Meisner, J.; Neuman, B.W.; Perez, M.; de la Torre, J.C.; Buchmeier, M.J. Mapping the landscape of the lymphocytic choriomeningitis virus stable signal peptide reveals novel functional domains. *J Virol* **2007**, *81*, 5649-5657, doi:10.1128/JVI.02759-06.

76. Burns, J.W.; Buchmeier, M.J. Protein-protein interactions in lymphocytic choriomeningitis virus. *Virology* **1991**, *183*, 620-629, doi:10.1016/0042-6822(91)90991-j.

77. Eschli, B.; Quirin, K.; Wepf, A.; Weber, J.; Zinkernagel, R.; Hengartner, H. Identification of an N-terminal trimeric coiled-coil core within arenavirus glycoprotein 2 permits assignment to class I viral fusion proteins. *J Virol* **2006**, *80*, 5897-5907, doi:10.1128/JVI.00008-06.

78. Cao, W.; Henry, M.D.; Borrow, P.; Yamada, H.; Elder, J.H.; Ravkov, E.V.; Nichol, S.T.; Compans, R.W.; Campbell, K.P.; Oldstone, M.B.A. Identification of α-Dystroglycan as a Receptor for Lymphocytic Choriomeningitis Virus and Lassa Fever Virus. *Science* **1998**, *282*, 2079-2081.

79. Kunz, S.; Rojek, J.M.; Kanagawa, M.; Spiropoulou, C.F.; Barresi, R.; Campbell, K.P.; Oldstone, M.B. Posttranslational modification of alpha-dystroglycan, the cellular receptor for arenaviruses, by the glycosyltransferase LARGE is critical for virus binding. *J Virol* **2005**, *79*, 14282-14296, doi:10.1128/JVI.79.22.14282-14296.2005.

80. Barresi, R.; Campbell, K.P. Dystroglycan: from biosynthesis to pathogenesis of human disease. *J Cell Sci* **2006**, *119*, 199-207, doi:10.1242/jcs.02814.

81. Jae, L.T.; Raaben, M.; Herbert, A.S.; Kuehne, A.I.; Wirchnianski, A.S.; Soh, T.K.; Stubbs, S.H.; Janssen, H.; Damme, M.; Saftig, P., et al. Virus entry. Lassa virus entry requires a trigger-induced receptor switch. *Science* **2014**, *344*, 1506-1510, doi:10.1126/science.1252480.

82. Goncalves, A.R.; Moraz, M.L.; Pasquato, A.; Helenius, A.; Lozach, P.Y.; Kunz, S. Role of DC-SIGN in Lassa virus entry into human dendritic cells. *J Virol* **2013**, *87*, 11504-11515, doi:10.1128/JVI.01893-13.

83. Shimojima, M.; Stroher, U.; Ebihara, H.; Feldmann, H.; Kawaoka, Y. Identification of cell surface molecules involved in dystroglycan-independent Lassa virus cell entry. *J Virol* **2012**, *86*, 2067-2078, doi:10.1128/JVI.06451-11.

84. Fedeli, C.; Torriani, G.; Galan-Navarro, C.; Moraz, M.L.; Moreno, H.; Gerold, G.; Kunz, S. Axl Can Serve as Entry Factor for Lassa Virus Depending on the Functional Glycosylation of Dystroglycan. *J Virol* **2018**, *92*, doi:10.1128/JVI.01613-17.

85. Brouillette, R.B.; Phillips, E.K.; Patel, R.; Mahauad-Fernandez, W.; Moller-Tank, S.; Rogers, K.J.; Dillard, J.A.; Cooney, A.L.; Martinez-Sobrido, L.; Okeoma, C., et al. TIM-1 Mediates Dystroglycan-Independent Entry of Lassa Virus. *J Virol* **2018**, *92*, doi:10.1128/JVI.00093-18.

86. Vela, E.M.; Zhang, L.; Colpitts, T.M.; Davey, R.A.; Aronson, J.F. Arenavirus entry occurs through a cholesterol-dependent, non-caveolar, clathrin-mediated endocytic mechanism. *Virology* **2007**, *369*, 1-11, doi:10.1016/j.virol.2007.07.014.

87. Oppliger, J.; Torriani, G.; Herrador, A.; Kunz, S. Lassa Virus Cell Entry via Dystroglycan Involves an Unusual Pathway of Macropinocytosis. *J Virol* **2016**, *90*, 6412-6429, doi:10.1128/JVI.00257-16.

88. Pasqual, G.; Rojek, J.M.; Masin, M.; Chatton, J.Y.; Kunz, S. Old world arenaviruses enter the host cell via the multivesicular body and depend on the endosomal sorting complex required for transport. *PLoS Pathog* **2011**, *7*, e1002232, doi:10.1371/journal.ppat.1002232.

89. Rojek, J.M.; Sanchez, A.B.; Nguyen, N.T.; de la Torre, J.C.; Kunz, S. Different mechanisms of cell entry by human-pathogenic Old World and New World arenaviruses. *J Virol* **2008**, *82*, 7677-7687, doi:10.1128/JVI.00560-08.

90. Li, S.; Sun, Z.; Pryce, R.; Parsy, M.L.; Fehling, S.K.; Schlie, K.; Siebert, C.A.; Garten, W.; Bowden, T.A.; Strecker, T., et al. Acidic pH-Induced Conformations and LAMP1 Binding of the Lassa Virus Glycoprotein Spike. *PLoS Pathog* **2016**, *12*, e1005418, doi:10.1371/journal.ppat.1005418.

91. Leroy, E.M.; Kumulungui, B.; Pourrut, X.; Rouquet, P.; Hassanin, A.; Yaba, P.; Delicat, A.; Paweska, J.T.; Gonzalez, J.P.; Swanepoel, R. Fruit bats as reservoirs of Ebola virus. *Nature* **2005**, *438*, 575-576, doi:10.1038/438575a.

92. Biek, R.; Walsh, P.D.; Leroy, E.M.; Real, L.A. Recent common ancestry of Ebola Zaire virus found in a bat reservoir. *PLoS Pathog* **2006**, *2*, e90, doi:10.1371/journal.ppat.0020090.

93. Pourrut, X.; Delicat, A.; Rollin, P.E.; Ksiazek, T.G.; Gonzalez, J.P.; Leroy, E.M. Spatial and temporal patterns of Zaire ebolavirus antibody prevalence in the possible reservoir bat species. *J Infect Dis* **2007**, *196 Suppl 2*, S176-183, doi:10.1086/520541.

94. Henao-Restrepo, A.M.; Longini, I.M.; Egger, M.; Dean, N.E.; Edmunds, W.J.; Camacho, A.; Carroll, M.W.; Doumbia, M.; Draguez, B.; Duraffour, S., et al. Efficacy and effectiveness of an rVSV-vectored vaccine expressing Ebola surface glycoprotein: interim results from the Guinea ring vaccination cluster-randomised trial. *The Lancet* **2015**, *386*, 857-866, doi:10.1016/s0140-6736(15)61117-5.

95. World Health Organization. Ebola Virus Disease. Availabe online: https://www.who.int/news-room/fact-sheets/detail/ebola-virus-disease (accessed on 23 June 2020).

96. Center for Disease Control and Prevention. Ebola (Ebola Virus Disease). Availabe online: https://www.cdc.gov/vhf/ebola/index.html (accessed on 23 June 2020).

97. Ellis, D.S.; Simpson, I.H.; Francis, D.P.; Knobloch, J.; Bowen, E.T.; Lolik, P.; Deng, I.M. Ultrastructure of Ebola virus particles in human liver. *J Clin Pathol* **1978**, *31*, 201-208, doi:10.1136/jcp.31.3.201.

98. Geisbert, T.W.; Jahrling, P.B. Differentiation of filoviruses by electron microscopy. *Virus Res* **1995**, *39*, 129-150, doi:10.1016/0168-1702(95)00080-1.

99. Beniac, D.R.; Melito, P.L.; Devarennes, S.L.; Hiebert, S.L.; Rabb, M.J.; Lamboo, L.L.; Jones, S.M.; Booth, T.F. The organisation of Ebola virus reveals a capacity for extensive, modular polyploidy. *PLoS One* **2012**, *7*, e29608, doi:10.1371/journal.pone.0029608.

100. Sanchez, A.; Kiley, M.P.; Holloway, B.P.; Auperin, D.D. Sequence analysis of the Ebola virus genome: organization, genetic elements, and comparison with the genome of Marburg virus. *Virus Res* **1993**, *29*, 215-240, doi:10.1016/0168-1702(93)90063-s.

101. Volchkov, V.E.; Becker, S.; Volchkova, V.A.; Ternovoj, V.A.; Kotov, A.N.; Netesov, S.V.; Klenk, H.D. GP mRNA of Ebola virus is edited by the Ebola virus polymerase and by T7 and vaccinia virus polymerases. *Virology* **1995**, *214*, 421-430, doi:10.1006/viro.1995.0052.

102. Sanchez, A.; Trappier, S.G.; Mahy, B.W.; Peters, C.J.; Nichol, S.T. The virion glycoproteins of Ebola viruses are encoded in two reading frames and are expressed through transcriptional editing. *Proc Natl Acad Sci U S A* **1996**, *93*, 3602-3607, doi:10.1073/pnas.93.8.3602.

103. Volchkova, V.A.; Feldmann, H.; Klenk, H.D.; Volchkov, V.E. The nonstructural small glycoprotein sGP of Ebola virus is secreted as an antiparallel-orientated homodimer. *Virology* **1998**, *250*, 408-414, doi:10.1006/viro.1998.9389.

104. Mehedi, M.; Falzarano, D.; Seebach, J.; Hu, X.; Carpenter, M.S.; Schnittler, H.J.; Feldmann, H. A new Ebola virus nonstructural glycoprotein expressed through RNA editing. *J Virol* **2011**, *85*, 5406-5414, doi:10.1128/JVI.02190-10.

105. Zhu, W.; Banadyga, L.; Emeterio, K.; Wong, G.; Qiu, X. The Roles of Ebola Virus Soluble Glycoprotein in Replication, Pathogenesis, and Countermeasure Development. *Viruses* **2019**, *11*, doi:10.3390/v11110999.

106. Volchkov, V.E.; Feldmann, H.; Volchkova, V.A.; Klenk, H.D. Processing of the Ebola virus glycoprotein by the proprotein convertase furin. *Proc Natl Acad Sci U S A* **1998**, *95*, 5762-5767, doi:10.1073/pnas.95.10.5762.

107. Manicassamy, B.; Wang, J.; Jiang, H.; Rong, L. Comprehensive analysis of ebola virus GP1 in viral entry. *J Virol* **2005**, *79*, 4793-4805, doi:10.1128/JVI.79.8.4793-4805.2005.

108. Sanchez, A.; Yang, Z.Y.; Xu, L.; Nabel, G.J.; Crews, T.; Peters, C.J. Biochemical analysis of the secreted and virion glycoproteins of Ebola virus. *J Virol* **1998**, *72*, 6442-6447.

109. Jeffers, S.A.; Sanders, D.A.; Sanchez, A. Covalent modifications of the ebola virus glycoprotein. *J Virol* **2002**, *76*, 12463-12472, doi:10.1128/jvi.76.24.12463-12472.2002.

110. Iraqi, M.; Edri, A.; Greenshpan, Y.; Kundu, K.; Bolel, P.; Cahana, A.; Ottolenghi, A.; Gazit, R.; Lobel, L.; Braiman, A., et al. N-Glycans Mediate the Ebola Virus-GP1 Shielding of Ligands to Immune Receptors and Immune Evasion. *Front Cell Infect Microbiol* **2020**, *10*, 48, doi:10.3389/fcimb.2020.00048.

111. Takada, A.; Fujioka, K.; Tsuiji, M.; Morikawa, A.; Higashi, N.; Ebihara, H.; Kobasa, D.; Feldmann, H.; Irimura, T.; Kawaoka, Y. Human macrophage C-type lectin specific for galactose and N-acetylgalactosamine promotes filovirus entry. *J Virol* **2004**, *78*, 2943-2947, doi:10.1128/jvi.78.6.2943-2947.2004.

112. Ning, Y.J.; Kang, Z.; Xing, J.; Min, Y.Q.; Liu, D.; Feng, K.; Wang, M.; Deng, F.; Zhou, Y.; Hu, Z., et al. Ebola virus mucin-like glycoprotein (Emuc) induces remarkable acute inflammation and tissue injury: evidence for Emuc pathogenicity in vivo. *Protein Cell* **2018**, *9*, 389-393, doi:10.1007/s13238-017-0471-x.

113. Dolnik, O.; Volchkova, V.; Garten, W.; Carbonnelle, C.; Becker, S.; Kahnt, J.; Stroher, U.; Klenk, H.D.; Volchkov, V. Ectodomain shedding of the glycoprotein GP of Ebola virus. *EMBO J* **2004**, *23*, 2175-2184, doi:10.1038/sj.emboj.7600219.

114. Escudero-Perez, B.; Volchkova, V.A.; Dolnik, O.; Lawrence, P.; Volchkov, V.E. Shed GP of Ebola virus triggers immune activation and increased vascular permeability. *PLoS Pathog* **2014**, *10*, e1004509, doi:10.1371/journal.ppat.1004509.

115. Radoshitzky, S.R.; Warfield, K.L.; Chi, X.; Dong, L.; Kota, K.; Bradfute, S.B.; Gearhart, J.D.; Retterer, C.; Kranzusch, P.J.; Misasi, J.N., et al. Ebolavirus delta-peptide immunoadhesins inhibit marburgvirus and ebolavirus cell entry. *J Virol* **2011**, *85*, 8502-8513, doi:10.1128/JVI.02600-10.

116. He, J.; Melnik, L.I.; Komin, A.; Wiedman, G.; Fuselier, T.; Morris, C.F.; Starr, C.G.; Searson, P.C.; Gallaher, W.R.; Hristova, K., et al. Ebola Virus Delta Peptide Is a Viroporin. *J Virol* **2017**, *91*, doi:10.1128/JVI.00438-17.

117. Volchkova, V.A.; Klenk, H.D.; Volchkov, V.E. Delta-peptide is the carboxy-terminal cleavage fragment of the nonstructural small glycoprotein sGP of Ebola virus. *Virology* **1999**, *265*, 164-171, doi:10.1006/viro.1999.0034.

118. Geisbert, T.W.; Hensley, L.E.; Larsen, T.; Young, H.A.; Reed, D.S.; Geisbert, J.B.; Scott, D.P.; Kagan, E.; Jahrling, P.B.; Davis, K.J. Pathogenesis of Ebola hemorrhagic fever in cynomolgus macaques: evidence that dendritic cells are early and sustained targets of infection. *Am J Pathol* **2003**, *163*, 2347-2370, doi:10.1016/S0002-9440(10)63591-2.

119. Tamhankar, M.; Gerhardt, D.M.; Bennett, R.S.; Murphy, N.; Jahrling, P.B.; Patterson, J.L. Heparan sulfate is an important mediator of Ebola virus infection in polarized epithelial cells. *Virol J* **2018**, *15*, 135, doi:10.1186/s12985-018-1045-0.

120. Alvarez, C.P.; Lasala, F.; Carrillo, J.; Muniz, O.; Corbi, A.L.; Delgado, R. C-type lectins DC-SIGN and L-SIGN mediate cellular entry by Ebola virus in cis and in trans. *J Virol* **2002**, *76*, 6841-6844, doi:10.1128/jvi.76.13.6841-6844.2002.

121. Simmons, G.; Reeves, J.D.; Grogan, C.C.; Vandenberghe, L.H.; Baribaud, F.; Whitbeck, J.C.; Burke, E.; Buchmeier, M.J.; Soilleux, E.J.; Riley, J.L., et al. DC-SIGN and DC-SIGNR bind ebola glycoproteins and enhance infection of macrophages and endothelial cells. *Virology* **2003**, *305*, 115-123, doi:10.1006/viro.2002.1730.

122. Zhao, D.; Han, X.; Zheng, X.; Wang, H.; Yang, Z.; Liu, D.; Han, K.; Liu, J.; Wang, X.; Yang, W., et al. The Myeloid LSECtin Is a DAP12-Coupled Receptor That Is Crucial for Inflammatory Response Induced by Ebola Virus Glycoprotein. *PLoS Pathog* **2016**, *12*, e1005487, doi:10.1371/journal.ppat.1005487.

123. Powlesland, A.S.; Fisch, T.; Taylor, M.E.; Smith, D.F.; Tissot, B.; Dell, A.; Pohlmann, S.; Drickamer, K. A novel mechanism for LSECtin binding to Ebola virus surface glycoprotein through truncated glycans. *J Biol Chem* **2008**, *283*, 593-602, doi:10.1074/jbc.M706292200.

124. Takada, A.; Watanabe, S.; Ito, H.; Okazaki, K.; Kida, H.; Kawaoka, Y. Downregulation of beta1 integrins by Ebola virus glycoprotein: implication for virus entry. *Virology* **2000**, *278*, 20-26, doi:10.1006/viro.2000.0601.

125. Kondratowicz, A.S.; Lennemann, N.J.; Sinn, P.L.; Davey, R.A.; Hunt, C.L.; Moller-Tank, S.; Meyerholz, D.K.; Rennert, P.; Mullins, R.F.; Brindley, M., et al. T-cell immunoglobulin and mucin domain 1 (TIM-1) is a receptor for Zaire Ebolavirus and Lake Victoria Marburgvirus. *Proc Natl Acad Sci U S A* **2011**, *108*, 8426-8431, doi:10.1073/pnas.1019030108.

126. Shimojima, M.; Takada, A.; Ebihara, H.; Neumann, G.; Fujioka, K.; Irimura, T.; Jones, S.; Feldmann, H.; Kawaoka, Y. Tyro3 family-mediated cell entry of Ebola and Marburg viruses. *J Virol* **2006**, *80*, 10109-10116, doi:10.1128/JVI.01157-06.

127. Brindley, M.A.; Hunt, C.L.; Kondratowicz, A.S.; Bowman, J.; Sinn, P.L.; McCray, P.B.; Quinn, K.; Weller, M.L.; Chiorini, J.A.; Maury, W. Tyrosine kinase receptor Axl enhances entry of Zaire ebolavirus without direct interactions with the viral glycoprotein. *Virology* **2011**, *415*, 83-94, doi:10.1016/j.virol.2011.04.002.

128. Dahlmann, F.; Biedenkopf, N.; Babler, A.; Jahnen-Dechent, W.; Karsten, C.B.; Gnirss, K.; Schneider, H.; Wrensch, F.; O'Callaghan, C.A.; Bertram, S., et al. Analysis of Ebola Virus Entry Into Macrophages. *J Infect Dis* **2015**, *212 Suppl 2*, S247-257, doi:10.1093/infdis/jiv140.

129. Hunt, C.L.; Kolokoltsov, A.A.; Davey, R.A.; Maury, W. The Tyro3 receptor kinase Axl enhances macropinocytosis of Zaire ebolavirus. *J Virol* **2011**, *85*, 334-347, doi:10.1128/JVI.01278-09.

130. Nanbo, A.; Imai, M.; Watanabe, S.; Noda, T.; Takahashi, K.; Neumann, G.; Halfmann, P.; Kawaoka, Y. Ebolavirus is internalized into host cells via macropinocytosis in a viral glycoprotein-dependent manner. *PLoS Pathog* **2010**, *6*, e1001121, doi:10.1371/journal.ppat.1001121.

131. Saeed, M.F.; Kolokoltsov, A.A.; Albrecht, T.; Davey, R.A. Cellular entry of ebola virus involves uptake by a macropinocytosis-like mechanism and subsequent trafficking through early and late endosomes. *PLoS Pathog* **2010**, *6*, e1001110, doi:10.1371/journal.ppat.1001110.

132. Amara, A.; Mercer, J. Viral apoptotic mimicry. *Nat Rev Microbiol* **2015**, *13*, 461-469, doi:10.1038/nrmicro3469.

133. Empig, C.J.; Goldsmith, M.A. Association of the caveola vesicular system with cellular entry by filoviruses. *J Virol* **2002**, *76*, 5266-5270, doi:10.1128/jvi.76.10.5266-5270.2002.

134. Bhattacharyya, S.; Warfield, K.L.; Ruthel, G.; Bavari, S.; Aman, M.J.; Hope, T.J. Ebola virus uses clathrin-mediated endocytosis as an entry pathway. *Virology* **2010**, *401*, 18-28, doi:10.1016/j.virol.2010.02.015.

135. Aleksandrowicz, P.; Marzi, A.; Biedenkopf, N.; Beimforde, N.; Becker, S.; Hoenen, T.; Feldmann, H.; Schnittler, H.J. Ebola virus enters host cells by macropinocytosis and clathrin-mediated endocytosis. *J Infect Dis* **2011**, *204 Suppl 3*, S957-967, doi:10.1093/infdis/jir326.

136. Simmons, G.; Rennekamp, A.J.; Chai, N.; Vandenberghe, L.H.; Riley, J.L.; Bates, P. Folate receptor alpha and caveolae are not required for Ebola virus glycoprotein-mediated viral infection. *J Virol* **2003**, *77*, 13433-13438, doi:10.1128/jvi.77.24.13433-13438.2003.

137. Sanchez, A. Analysis of filovirus entry into vero e6 cells, using inhibitors of endocytosis, endosomal acidification, structural integrity, and cathepsin (B and L) activity. *J Infect Dis* **2007**, *196 Suppl 2*, S251-258, doi:10.1086/520597.

138. Chandran, K.; Sullivan, N.J.; Felbor, U.; Whelan, S.P.; Cunningham, J.M. Endosomal proteolysis of the Ebola virus glycoprotein is necessary for infection. *Science* **2005**, *308*, 1643-1645, doi:10.1126/science.1110656.

139. Schornberg, K.; Matsuyama, S.; Kabsch, K.; Delos, S.; Bouton, A.; White, J. Role of endosomal cathepsins in entry mediated by the Ebola virus glycoprotein. *J Virol* **2006**, *80*, 4174-4178, doi:10.1128/JVI.80.8.4174-4178.2006.

140. Carette, J.E.; Raaben, M.; Wong, A.C.; Herbert, A.S.; Obernosterer, G.; Mulherkar, N.; Kuehne, A.I.; Kranzusch, P.J.; Griffin, A.M.; Ruthel, G., et al. Ebola virus entry requires the cholesterol transporter Niemann-Pick C1. *Nature* **2011**, *477*, 340-343, doi:10.1038/nature10348.

141. Cote, M.; Misasi, J.; Ren, T.; Bruchez, A.; Lee, K.; Filone, C.M.; Hensley, L.; Li, Q.; Ory, D.; Chandran, K., et al. Small molecule inhibitors reveal Niemann-Pick C1 is essential for Ebola virus infection. *Nature* **2011**, *477*, 344-U122, doi:10.1038/nature10380.

142. Wool-Lewis, R.J.; Bates, P. Characterization of Ebola Virus Entry by Using Pseudotyped Viruses: Identification of Receptor-Deficient Cell Lines. *j Virol* **1998**, *72*, 3155-3160.

143. Acciani, M.D.; Lay-Mendoza, M.F.; Havranek, K.E.; Duncan, A.M.; Iyer, H.; Linn, O.L.; Brindley, M.A. Ebola virus requires phosphatidylserine scrambling activity for efficient budding and optimal infectivity. *bioRxiv* **2020**, 10.1101/2020.03.16.994012, 2020.2003.2016.994012, doi:10.1101/2020.03.16.994012.

144. Ono, N.; Tatsuo, H.; Hidaka, Y.; Aoki, T.; Minagawa, H.; Yanagi, Y. Measles viruses on throat swabs from measles patients use signaling lymphocytic activation molecule (CDw150) but not CD46 as a cellular receptor. *J Virol* **2001**, *75*, 4399-4401, doi:10.1128/JVI.75.9.4399-4401.2001.

145. Buchholz, U.J.; Finke, S.; Conzelmann, K.K. Generation of bovine respiratory syncytial virus (BRSV) from cDNA: BRSV NS2 is not essential for virus replication in tissue culture, and the human RSV leader region acts as a functional BRSV genome promoter. *J Virol* **1999**, *73*, 251-259.

146. Acciani, M.; Alston, J.T.; Zhao, G.; Reynolds, H.; Ali, A.M.; Xu, B.; Brindley, M.A. Mutational Analysis of Lassa Virus Glycoprotein Highlights Regions Required for Alpha-Dystroglycan Utilization. *J Virol* **2017**, *91*, doi:10.1128/JVI.00574-17.

147. Salvador, B.; Zhou, Y.; Michault, A.; Muench, M.O.; Simmons, G. Characterization of Chikungunya pseudotyped viruses: Identification of refractory cell lines and demonstration of cellular tropism differences mediated by mutations in E1 glycoprotein. *Virology* **2009**, *393*, 33-41, doi:10.1016/j.virol.2009.07.013.

148. Ramakrishnan, M.A. Determination of 50% endpoint titer using a simple formula. *World J Virol* **2016**, *5*, 85-86, doi:10.5501/wjv.v5.i2.85.

149. Baer, A.; Kehn-Hall, K. Viral concentration determination through plaque assays: using traditional and novel overlay systems. *J Vis Exp* **2014**, 10.3791/52065, e52065, doi:10.3791/52065.

150. Timm, A.; Yin, J. Kinetics of virus production from single cells. *Virology* **2012**, *424*, 11-17, doi:10.1016/j.virol.2011.12.005.

151. Jae, L.T.; Brummelkamp, T.R. Emerging intracellular receptors for hemorrhagic fever viruses. *Trends Microbiol* **2015**, *23*, 392-400, doi:10.1016/j.tim.2015.04.006.

152. Abraham, G.; Banerjee, A.K. Sequential transcription of the genes of vesicular stomatitis virus. *Proc Natl Acad Sci U S A* **1976**, *73*, 1504-1508, doi:10.1073/pnas.73.5.1504.

153. Rose, J.K.; Gallione, C.J. Nucleotide sequences of the mRNA's encoding the vesicular stomatitis virus G and M proteins determined from cDNA clones containing the complete coding regions. *J Virol* **1981**, *39*, 519-528.

154. Auperin, D.D.; McCormick, J.B. Nucleotide sequence of the Lassa virus (Josiah strain) S genome RNA and amino acid sequence comparison of the N and GPC proteins to other arenaviruses. *Virology* **1989**, *168*, 421-425, doi:10.1016/0042-6822(89)90287-0.

155. Rejman, J.; Oberle, V.; Zuhorn, I.S.; Hoekstra, D. Size-dependent internalization of particles via the pathways of clathrin- and caveolae-mediated endocytosis. *Biochem J* **2004**, *377*, 159-169, doi:10.1042/BJ20031253.

156. Rossman, J.S.; Leser, G.P.; Lamb, R.A. Filamentous influenza virus enters cells via macropinocytosis. *J Virol* **2012**, *86*, 10950-10960, doi:10.1128/JVI.05992-11.

157. Jemielity, S.; Wang, J.J.; Chan, Y.K.; Ahmed, A.A.; Li, W.; Monahan, S.; Bu, X.; Farzan, M.; Freeman, G.J.; Umetsu, D.T., et al. TIM-family proteins promote infection of multiple enveloped viruses through virion-associated phosphatidylserine. *PLoS Pathog* **2013**, *9*, e1003232, doi:10.1371/journal.ppat.1003232.

158. Holbrook, M.R.; Brunton, B.; Rogers, K.; Phillips, E.K.; Brouillette, R.B.; Bouls, R.; Butler, N.S.; Maury, W. TIM-1 serves as a receptor for Ebola virus in vivo, enhancing viremia and pathogenesis. *PLOS Neglected Tropical Diseases* **2019**, *13*, doi:10.1371/journal.pntd.0006983.

159. Kawashima, K.D.; Suarez, L.A.; Labayo, H.K.; Liles, V.R.; Salvoza, N.C.; Klinzing, D.C.; Daroy, M.L.; Matias, R.R.; Natividad, F.F. Complete genome sequence of chikungunya virus isolated in the Philippines. *Genome Announc* **2014**, *2*, doi:10.1128/genomeA.00336-14.

160. Hoornweg, T.E.; van Duijl-Richter, M.K.S.; Ayala Nunez, N.V.; Albulescu, I.C.; van Hemert, M.J.; Smit, J.M. Dynamics of Chikungunya Virus Cell Entry Unraveled by Single-Virus Tracking in Living Cells. *J Virol* **2016**, *90*, 4745-4756, doi:10.1128/JVI.03184-15.

161. Hulseberg, C.E.; Feneant, L.; Szymanska, K.M.; White, J.M. Lamp1 Increases the Efficiency of Lassa Virus Infection by Promoting Fusion in Less Acidic Endosomal Compartments. *mBio* **2018**, *9*, doi:10.1128/mBio.01818-17.

162. Simmons, J.A.; D'Souza, R.S.; Ruas, M.; Galione, A.; Casanova, J.E.; White, J.M. Ebolavirus Glycoprotein Directs Fusion through NPC1+ Endolysosomes. *J Virol* **2016**, *90*, 605-610, doi:10.1128/JVI.01828-15.